AREA 2: Novel Materials for Robust Repair of Leaky Wellbores in CO_2 Storage Formations

CONTRACT NO. DE-FE0009299

Project Period: 10/1/2012-1/31/2016
FINAL TECHNICAL REPORT
Submission Date: April 30, 2016

Authors
Matthew T. Balhoff
Shayan Tavassoli
Jostine Fei Ho
Department of Petroleum and Geosystems Engineering
The University of Texas at Austin
1 University Station C0300
Austin, TX 78712-0228
Phone: (512) 471 3246
Email: balhoff@mail.utexas.edu
s.tavassoli@mail.utexas.edu

DUNS Number: 170230239

Prepared for
U.S. Department of Energy - NETL
3610 Collins Ferry Road
P.O. Box 880
Morgantown, WV 26508

Acknowledgment: "This material is based upon work supported by the Department of Energy under Award Number DE-FE0009299."

ABSTRACT

The potential leakage of hydrocarbon fluids or CO_2 out of subsurface formations through wells with fractured cement or debonded microannuli is a primary concern in oil and gas production and CO_2 storage. The presence of fractures in a cement annulus with apertures on the order of 10–300 microns can pose a significant leakage danger with effective permeability in the range of 0.1–1 mD (millidarcy). Leakage pathways with small apertures are often difficult to repair using conventional oilfield cement, thus a low-viscosity sealant that can be easily placed into these fractures while providing an effective seal is desired. The development of a novel application using pH-triggered polymeric sealants could potentially be the solution to plugging these fractures and that was the research aim of this study.

The application is based on the transport and reaction of a low-pH poly(acrylic acid) polymer through fractures in strongly alkaline cement. The pH-sensitive microgels viscosify upon neutralization with cement to become highly swollen gels with substantial yield stress that can block fluid flow. Experiments in a cement fracture determined the effects of the viscosification and gel deposition via real-time visual observation and measurements of pressure gradient and effluent pH. While the pH-triggered gelling mechanism and rheology measurements of the neutralized polymer gel show promising results, the polymer solution in contact with cement undergoes an undesirable reaction known as polymer syneresis. Syneresis is caused by the release of calcium cation from cement that collapses the polymer network. Syneresis produces an unstable calcium-precipitation byproduct that is detrimental to the strength and stability of the gel in place. As a result, gel-sealed leakage pathways that subjected to various degrees of syneresis often failed to hold back pressures.

Several chemicals were studied to inhibit polymer syneresis and tested for pretreatment of cement cores to remove calcium and prevent syneresis during polymer placement. A chelating agent, sodium triphosphate ($Na_5P_3O_{10}$), was found to successfully eliminate syneresis without compromising the injectivity of polymer solution during placement. Polymer gel strength is determined by recording the maximum holdback pressure gradients during liquid breakthrough tests after various periods of pretreatment and polymer shut-in time. Cores pretreated with $Na_5P_3O_{10}$ successfully held up to an average of 80 psi/ft, which is significantly greater than the expected threshold value of about 0.1-5 psi/ft required to prevent flow in a typical CO_2 leakage scenario. The use of such inexpensive, pH-triggered poly-acrylic acid polymer allows long-term robust seal of leaky wellbores under high pH conditions.

TABLE OF CONTENTS

EXECUTIVE SUMMARY

The potential leakage of hydrocarbon fluids or CO_2 out of subsurface formations through wells with fractured cement or debonded microannuli is a primary concern in oil and gas production and CO_2 storage. Traditionally, these fractures are repaired with cement squeeze operations, in which new cement is injected through perforations created in the casing near the suspected source of leakage to achieve proper zonal isolation. Fractures or leakage pathways with small apertures are often difficult for oilfield cement to repair because the cement slurry is potentially screened out from dispersing fluid and cannot enter the fractures. Therefore, squeeze cementing is often unsuccessful, and can result in a waste of rig time and escalation of costs. A novel application using pH-sensitive microgel dispersion is developed here as a solution to the disadvantageous of remediation workovers using conventional oilfield cement. The application is based on the reaction of a low-pH poly(acrylic acid) polymer that can be easily injected into small apertures and can develop substantial yield stress when passing through strongly alkaline cement fractures. While the pH–trigger mechanism and rheology show promising results, an unexpected phenomenon, known as polymer syneresis, produced a byproduct that was proven to compromise the seal of the injected gel in place.

The objective of this project is to develop a pH-triggered polymer (microgel) formula and injection technique to effectively seal cement fractures and achieve long-term blockage. We developed experimental procedures and configurations to conduct experiments to test polymer capability to block leakage pathways. Several experiments were performed to evaluate the polymer resistivity using brine injection. Although many rheology tests have confirmed the ability of the polymer in developing significant yield stresses, an unexpected reaction occurred when tests were done with cement. Calcium ions contained in the cement leached out into the fracture and reacted with the polymer dispersion to form calcium precipitates. This reaction causes polymer syneresis in which water is expelled from the gel structure causing an irreversible shrinkage in its volume. Syneresed gel is shown to be detrimental to the strength and long-term stability of the gel placement. This study focuses on understanding the development of polymer viscosity and identifying the main components of syneresis. Several chemicals were studied to inhibit syneresis and tested as either polymer additives or cement pretreatment in cement fracture corefloods. The chemical inhibitors and its applications were then selected based on not only their ability to eliminate syneresis, but also their reaction with polymer during injection and subsequent development of gel yield stress in cement fractures. The ease of polymer injection and the resulting gel strength were the key metrics for determining the feasibility of the application. Cores pretreated with a chelating agent, known as sodium triphosphate ($Na_5P_3O_{10}$), showed good injectivity during polymer placement and significant improved sealing performance during water breakthrough tests. In addition, the pretreatment procedure greatly reduced the calcium content in the cement and prevented polymer syneresis of the sealing gel.

The governing equations of the process are discussed and modeling procedure is explained. Polymer gel rheology and behavior were measured in laboratory experiments and formulations were developed to predict its behavior at different conditions. The simulation model was used to study the gelant flow through the fracture. The model was validated against laboratory

experiments. Several experiments were performed to evaluate the polymer resistivity using acidic brine breakthrough tests. Additional experiments were conducted using CO_2 (low/high pressure) breakthrough tests. The resulting gel-in-place using pretreated cores provided longer periods of effective seal and held pressure gradients orders of magnitude higher than just a few psi/ft compared to gel placed in un-treated cores. Furthermore, the comparison of holdback pressure gradients between designed corefloods indicated improvement in gel strength as fracture aperture is decreased and polymer shut-in time is increased.

Field wellbore prototype leakage study is performed in this study. Cement annulus bench tests were conducted using the setup analogous to real cement wellbores in shallow formations. The tests were done to evaluate the capability of pH-triggered gels to stop bulk phase CO_2 leaks. Several experiments and sensitivity analyses were performed to understand the effects of various parameters on the performance of polymer gel and to optimize the formulation in order to improve its performance. With proper cement pretreatment, the pH-triggered polymer-gel system has been seen to effectively plug small fractures and have valuable applications for long-term robust seal in leaky wellbores. Although harsher reservoir conditions have yet been extensively tested, the lab-scale testing shows promising application for field-scale tests in shallow wells.

INTRODUCTION

The leakage of fluids through fractured wells is a primary concern in hydrocarbon recovery and carbon sequestration (Dusseault et al. 2000). In the geologic storage of anthropogenic carbon dioxide leakage of buoyant CO_2 plumes from storage reservoirs into shallower formations, aquifers, or the surface can occur. Man-made wells drilled through these formations present a potential leakage pathway for stored CO_2 as the cement binding the well to the earth develops fractures or as debonded microannuli form between cement and surrounding materials over time (Watson et al. 2007). Wellbore cement can develop leaks, either by chemical attack from formation fluids or by mechanical stressing causing by pressure or thermal cycling resulting from the production of hot reservoir fluids or injection of relatively cold surface fluids (Milanovic and Smith 2005). The presence of an annular gap and/or fractures with apertures on the order of 0.01–0.3 mm leads to a significant increase in effective permeability in the range of 0.1–1 mD (Um et al. 2014). Typically, wells with poor cementing or suspected leaks are repaired with a cement-squeeze, in which new cement is injected through perforations created in the casing near the suspected source or leakage pathway to fill the pathway. However, fractures or leakage pathways with small apertures are often difficult for oilfield cement to repair, as the cement slurry is potentially screened out from dispersing fluid and cannot enter the fracture. Therefore a low-viscosity sealant is desired that can enter these leakage pathways easily and provide a robust seal.

Pressure elevation within a CO_2 storage reservoir during injection is unlikely to exceed ~1,000 psi above hydrostatic, and leakage pathways must extend through 10s to 100s of ft of overlying caprock, making gradients of a few psi/ft possible. After injection ends, the driving force decreases to the gradient due to buoyancy, which is about 0.2 psi/ft for brine and supercritical CO_2 densities at typical storage reservoir conditions. For example, if CO_2 is rising through a leak due to buoyancy, the gradient will be $\Delta\rho g$ (ρ is the density and g is the gravitational constant), which is 0.2 psi/ft to 0.4 psi/ft depending on the depth. If injection has increased the pressure in the brine phase by 500 psi above the initial (hydrostatic) reservoir pressure and the leakage path is through an overlying seal of thickness 100 ft, then the gradient would be 5 psi/ft. Thus, if a material which has an almost water-like viscosity during its injection into the leakage pathway but viscosifies (and exhibits a desired yield stress) after a certain residence time, such a material would be useful for stopping CO_2 or brine from flowing. For a conduit with an aperture of 200 microns, the presence of a fluid with a yield stress of 100 Pa is sufficient to prevent fluid flow at pressure gradients up to 21 psi/ft. Such gradients are much larger than the aforementioned driving forces expected in the vertical direction along an existing wellbore during and after geologic sequestration of CO_2.

A yield stress fluid is a non-Newtonian fluid that does not flow below a critical applied stress, effectively acting as a solid (Barnes 1999). Yield stress is often measured dynamically in a rheometer by extrapolation to the y-intercept of a stress versus shear rate curve or static tests such as creep (Cloitre et al. 2003) or vane. There is some debate over whether a theoretical yield stress actually exists (Barnes 1999), but from a practical standpoint many fluids exhibit the characteristics of a yield-stress fluid. Examples of yield stress fluids include certain foodstuffs, muds, and gels (Gutowski et al. 2012). Empirical models such as the Bingham, Herschel-Bulkley, and Casson models are often fit to rheological data of shear stress versus shear rate with good accuracy.

A class of poly(acrylic acid) polymers known commercially as Carbopol® are pH-sensitive microgels and swell/thicken upon neutralization to become bulk gels with substantial yield stress of over 100 Pa (Huh et al. 2005). A schematic of pH-triggered gelling mechanism with injection of the polymer into a cement fracture is illustrated in **Fig. 1**. The main hydration product of interest in cement is calcium hydroxide, $Ca(OH)_2$, known as portlandite. The hydrated cement is highly alkaline with a pH of nearly 13. The cement, having a sufficient neutralization capacity to induce the pH transition for gel formation, no additives is needed for this application, nor would the treatment design have to account for the complexity of time/temperature/composition sensitive agents for gelation, such as polymer crosslinkers. Hence this polymer is potentially useful for repairing leakage pathways in oilfield cement, especially those that are too narrow to be easily treated by squeeze cementing. **Fig. 2** is an illustration of the leakage problem commonly seen in old cement wellbores and the remedial procedure using the pH-triggered polymer gel.

The material tested in this work (Carbopol® 934) has been one of the most widely used thickening and gelling agents for various commercial applications for the last fifty years. It is commonly used by rheologists and chemical engineers because of its versatility in imparting extreme non-Newtonian properties without excessive elasticity but highly shear thinning (Roberts and Barnes, 2001). One benefit to end-users is that this material is well-studied, inexpensive, and commercially available in quantity. Another benefit is that such yield stress fluids become more effective as the fracture they occupy becomes narrower. This is because the pressure gradient that the gel will withstand is inversely proportional to fracture aperture. Hence the leaks that are hardest to repair with cement squeezing will be the easiest to repair with this gel.

In this work, the polymer microgel dispersions are tested for ease of placement into cement-walled fractures and gel strength in holding back pressure after the reaction with cement. Laboratory experiments involved injecting various unswollen polymer microgel dispersions (typically starting at pH 2 to 2.5) into constructed cement fractures, that resembles a slit geometry, while measuring injection pressure and the pH of the polymer effluent to quantify the chemical reactions taking place and the induced viscosity changes. The viscosification of a fluid during flow in a slit will cause viscous fingering of the low viscosity fluid through the higher viscosity fluid in a self-reinforcing manner. The fingering effect was shown in Helfrich's (1995) study on magma flow in a thin slit, during which the magma loses heat to the slot walls and thus increases its viscosity. High temperature, low viscosity magma fingers through the cool, high viscosity magma, resulting in flow channels that carry hot fluid quickly through the fracture, even though the original flow field was uniform. This is analogous to the present application: the injected fluid reacts with alkali minerals at the slit wall and viscosifies. Thus subsequently injected fluid near the inlet will tend to preferentially flow in small "fingers" through the more viscous fluid downstream, establishing a channel/flow path. For a constant volumetric injection rate at the inlet, the local flow velocities in the channel are larger than in the original uniform flow field, resulting in less fluid/wall reaction, while the flow velocities outside of the channel are smaller, resulting in more fluid/wall interaction and therefore more viscosification.

The objective of this work is to evaluate the strongly coupled reactive transport problem in a fracture and to investigate the competing effects of fluid viscosification and solid deposition during flow. Ease of polymer gel placement and verification of long-term gel strength and stability are

the important factors in designing the polymer dispersion and its transportation in cement fractures. The objectives of this study were completed by the following tasks:

(1) Systematical investigation of the polymer gel resistance in fracture cement cores. We developed experimental procedures and configurations to conduct experiments to test the capability of the polymer gel to block leakage pathways.

(2) Preliminary evaluation of capability of pH-triggered gels to stop brine leaks. Several experiments were performed to evaluate the polymer gel resistivity using brine injection.

(3) Modeling reactive transport of acidity (pH) in cement fractures. The governing equations of the process are discussed and modeling procedure is explained.

(4) Modeling propagation of low pH gelant through typical leakage pathways and onset of gelation after placement. The simulation model was used to study the gelant flow through the fracture. The model was validated against laboratory experiments.

(5) Evaluation of capability of pH-triggered gels to stop leaks of acidic brine. Several experiments were performed to evaluate the polymer resistivity using acidic brine breakthrough tests. Additional experiments were conducted using CO_2 (low/high pressure) breakthrough tests.

(6) Formulation of model of gelant viscosity and gel yield stress for typical field conditions developed. Polymer gel rheology and behavior were measured in laboratory experiments and formulations were developed to predict its behavior at different conditions.

(7) Field wellbore prototype leakage study. Cement annulus bench tests were conducted using the setup analogous to real cement wellbores in shallow formations. The tests were done to evaluate the capability of pH-triggered gels to stop bulk phase CO_2 leaks.

(8) Optimization of the polymer formulation. Several experiments and sensitivity analyses were performed to understand the effects of various parameters on the performance of polymer gel and to optimize the formulation in order to improve its performance.

The remainder of the report describes the methods and results of these tasks. This is followed by the project summary and conclusions.

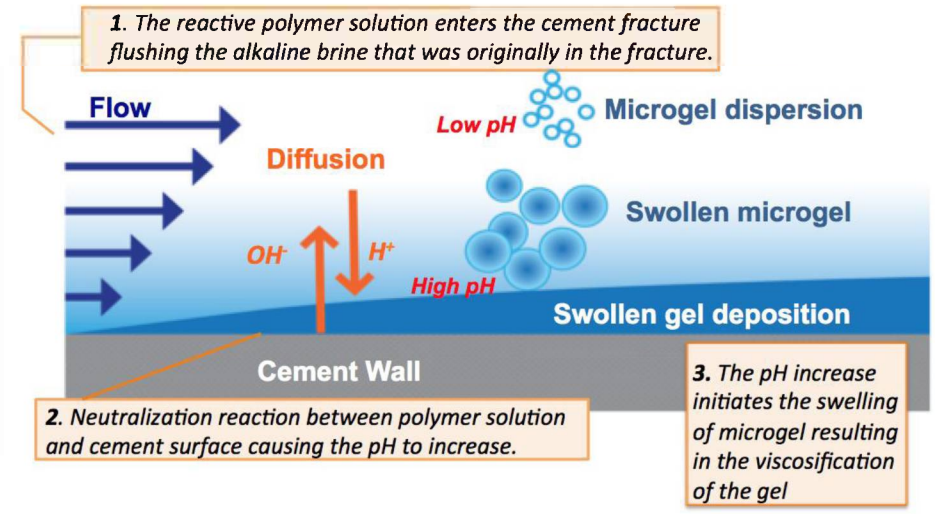

Fig. 1 – An illustration of the reaction between the pH-triggered microgel dispersion and the cement fracture. The microgel dispersion can be injected easily, much like water, into cement fracture starting at low pH. The pH and volume of the microgel dispersion increases while OH- ions leach out of the alkaline cement walls to neutralize the solution resulting in the viscosification of the gel. Swollen gel is then deposited in the cement fracture exhibiting behaviors of a semi-solid that can be used to seal leakage pathways of the cement fracture (Ho et al. 2015).

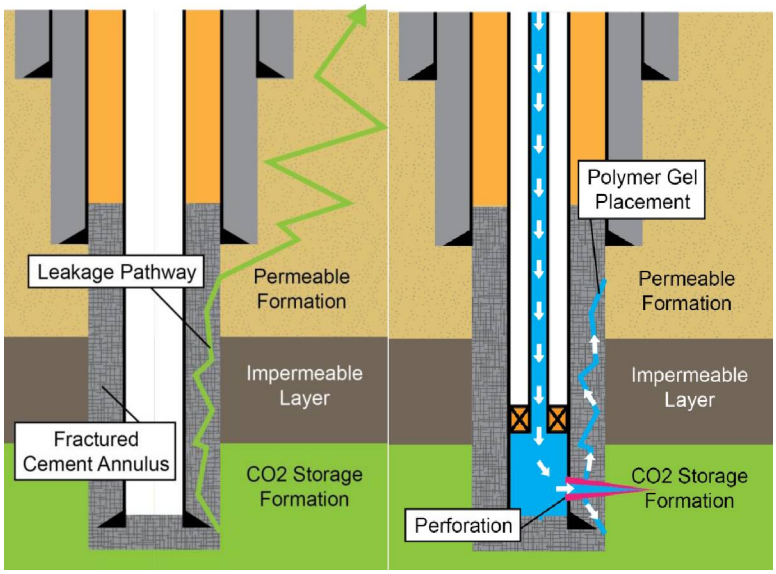

Fig. 2 – Leakage pathway in the fractured cement annulus (left) and polymer gel placement through perforation to seal the leakage (right) (Ho et al. 2015).

DETAILS

In this Details section, experimental methods are discussed first. This is followed by results and discussions. Finally, conclusions of the work are summarized.

1 Methods

In this section, we explain in details the rheological study of polymer gelant, coreflood experiments, cement annulus bench tests, and modeling.

1.1 RHEOLOGICAL STUDY OF POLYMER GELANT

Flow curve, the plot of shear stress versus shear rate is used extensively in rheology studies. Important parameters like yield stress, consistency index and power law index could be extracted from flow curve from which the behavior of the material could be predicted. For our application, yield stress can be used to see if the gelant can withstand against the pressure gradient induced by brine containing dissolved CO_2. Consistency index and power law index, the two other parameters would be used to model the non-Newtonian viscosity behavior of gelant in terms of pH, polymer concentration, shear rate, salinity, calcium concentration, and temperature.

The rheology of gelant is measured in different ways. With rheology, the behavior of the polymer gel could be predicted. By measuring rheological properties, we can figure out if the polymer gel can meet the requirements for stopping CO_2 leakage in leaky wellbores.

We developed a method to measure shear rate in a much broader range, especially for low shear rate values. For shear rate values of 1 1/s and higher, the stress ramp method was used to plot shear stress against shear rate. For the data points close to yield stress, the long term creep test was the best option (Shafiei et al. 2016). Combining these two methods gave us a smooth curve which fitted well into Herschel-Bulkley model.

1.1.1 Polymer gelant

The aqueous dispersion of unswollen microgel was prepared using Carbopol® 934, obtained from ARC Products Inc. (a product of The Lubrizol Co.). Carbopol® 934 was chosen for having the highest yield stress among the various polymer microgels tested (Carbopol® 1342, 940, 941, 934, Ultrez 10 and Ultrez 20). The mixtures were prepared using 3 wt% polymer in salinity range of 0 - 0.5 wt% NaCl. The dispersion was stirred for up to 24 hours, insuring proper polymer hydration.

1.1.2 Methodology and materials

Carbopol 934, DI water and NaOH 1M was used to make samples. We created a vortex in a large beaker with a magnetic stir bar and added polymer powder in small quantities to the center of the

vortex. The beaker was covered and stirred for 24 hours to ensure the polymer was fully hydrated. After adding 1M sodium hydroxide (NaOH) solution, the dispersion was mixed. We waited 20 minutes and then measured the pH. Due to increase in viscosity which caused by addition of NaOH, the diffusion could be slowed down. So by measuring the pH at different times we found the pH needs some time to be stable. The time required for pH to be stable is around 20 minutes but we waited long enough and read the final pH after 24 hours. As the viscosity of gel is high, the air could trap between gel particles during the mixing process. We centrifuged samples at 2,000 rpm for 10 minutes to eliminate the bubbles.

The rheology measurements were conducted using AR-G2 stress controlled rheometer (**Fig. 3**). The flat parallel plate geometry was selected (**Fig. 3**). To eliminate slippage artefact, we glued a piece of sandpaper with grit 80 to both plates (**Fig. 4**).

Fig. 3 – AR-G2 stress-controlled rheometer (left) and parallel plate geometry (right) (TA Instrument Co).

Fig. 4 – Geometry and Peltier modified with sandpaper to eliminate the slippage.

Stress was ramped and shear rate was measured. To avoid solvent evaporation, solvent trap was used in all of the experiments (**Fig. 5**). For data points close to the yield stress, creep test was conducted at a constant shear stress. In our experiments, shear rate was measured versus time until shear rate leveled off, which stands for the equilibrium point. The equilibrium shear rate would be

considered as one of the data points required to plot flow curve (plot of shear stress vs. shear rate). We conducted our experiments for a given pH=4.5 and different concentrations of polymer. **Fig. 6** shows the flow curve for polymer concentration of 0.5 wt. % at pH=4.5. We created the same curves for polymer concentrations of 1.0, 1.5, 2.0, 2.5 and 3.0 wt. %. The pH was kept at 4.5 for all the measurements.

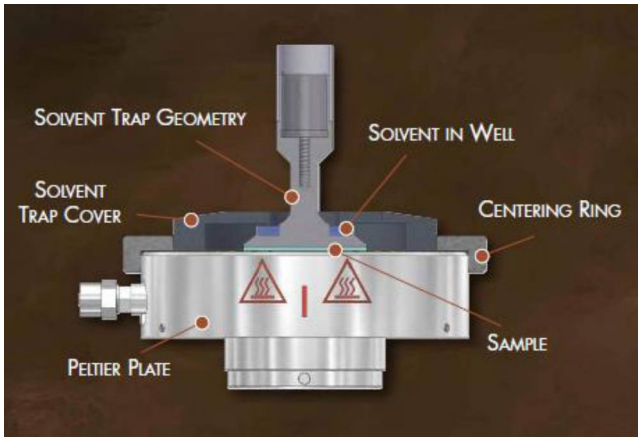

Fig. 5 – Solvent trap system (TA Instrument Co).

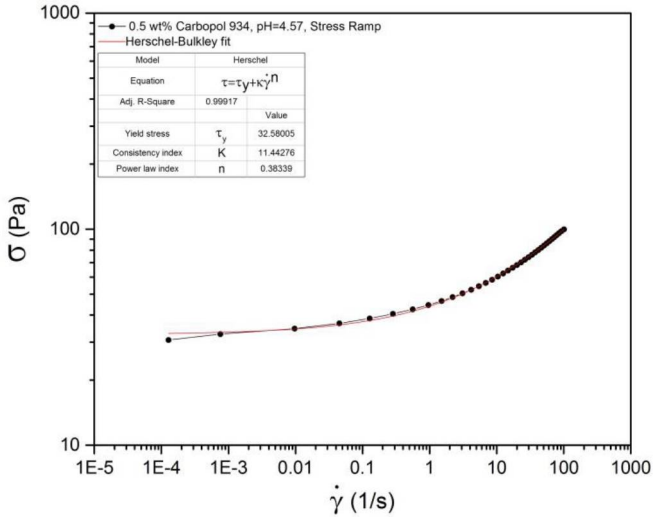

Fig. 6 – Shear stress versus shear rate for Carbopol 934, 0.5 wt. %.

From flow curve, important parameters like yield stress, consistency index and power law index could be obtained. As an example for 0.5 wt. % polymer concentration with pH=4.57, the yield stress of 32.6 Pa, K=11.4 and n=0.38 could be estimated which is shown in **Fig. 6**. The experimental data shown in flow curves, fitted very well into Herschel-Bulkley model. The model could be expressed by Eq. 1.

$$\sigma = \sigma_y + K\dot{\gamma}^n \ , \tag{1}$$

where σ, σ_y, K, $\dot{\gamma}$ and n are the shear stress, yield stress, consistency index, shear rate, and power law index, respectively. We conducted strain sweep experiment and plotted shear stress versus

strain. In this experiment the constant frequency of 0.1 Hz was applied for a range of strain values. From this graph we could obtain yield stress as well. **Fig. 7** shows the plotted data for 0.5 wt. % polymer concentration at pH=4.57. The yield stress was obtained from this plot at the intersect point of the trend lines with the value of 31.5 Pa in this case.

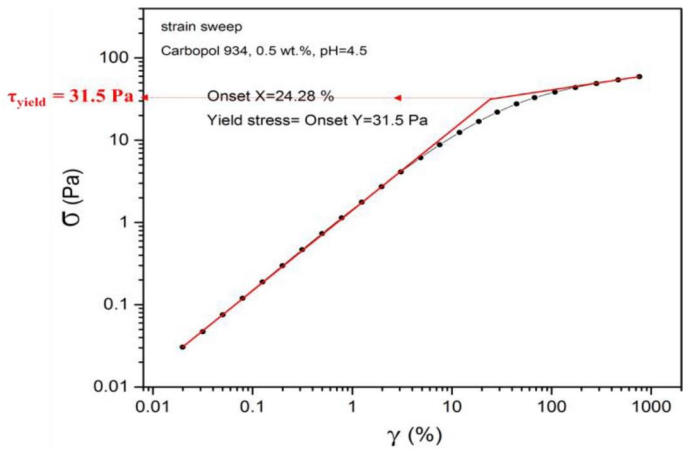

Fig. 7 – Shear stress versus shear rate for Carbopol 934, 0.5 wt. %.

By comparing Figs. 6 and 7, we found that there is a good agreement between the two methods in obtaining the yield stress of the polymer gel. As the strain sweep method takes a shorter time to complete, it could be used for the quick estimation of yield stress values.

1.1.3 Polymer rheology

The injection of pH-triggered polymer gel into cement fractures exhibits both viscosification and depositional effects that influence the flow rate or injection pressure during flow; these phenomena have been observed in past laboratory experiments (Patterson 2014). The polymer gel is seen to have a yield stress and shear thinning behavior. The yield stress exhibited is analogous to that of a solid material meaning that it does not flow below a critical applied stress (Barnes 1999). Shear thinning is seen in injection experiments where viscosity decreases while injection rate is increased. When a shear thinning fluid also possesses a yield stress, the low flow regions in which the shear stress is less than the yield stress will either exhibit plug flow or no flow.

Sealants exhibiting behaviors of a semi-solid that can be used to seal leakage pathways in cement fracture are ideal candidates. A class of poly(acrylic acid) polymers known commercially as Carbopol® are pH-sensitive microgels and swell/thicken upon neutralization to become bulk gels with substantial yield stress of over 100 Pa (Huh et al. 2005). Carbopol® 934 has been one of the most widely used thickening and gelling agents for various commercial applications for the last fifty years. This polymer is commonly used by rheologists and chemical engineers because of its versatility in imparting extreme non-Newtonian properties without excessive elasticity but highly shear thinning (Roberts and Barnes 2001; Shafiei et al. 2016).

1.2 COREFLOOD EXPERIMENTS

In this section, we provide the details on coreflood experiments. First, we present the materials used in the experiments. Then, we discuss the core preparation used in the experiments. Finally, we provide the experimental procedure and setup for various laboratory experiments. Please refer to Ho et al. (2015) and Ho (2015) for more details on these experiments.

1.2.1 Materials

The material tested (Carbopol® 934) has been one of the most widely used thickening and gelling agents for various commercial applications for the last fifty years. It is commonly used by rheologists and chemical engineers because of its versatility in imparting extreme non-Newtonian properties without excessive elasticity but highly shear thinning (Roberts and Barnes 2001). One benefit to end-users is that this material is well-studied, inexpensive, and commercially available in quantity. Another benefit is that such yield stress fluids become more effective as the fracture they occupy becomes narrower. This is because the pressure gradient that the gel will withstand is inversely proportional to fracture aperture. Hence, the leaks that are hardest to repair with cement squeezing will be the easiest to repair with this gel.

Chelating agents are commonly used as syneresis inhibitors for polymer applications in hard formation water (Albonico and Lockhart 1997). These chemicals can selectively remove metal ions, such as Ca^{2+} and Mg^{2+} by binding them to its molecule. Once bound, the metals are unable to react in undesirable ways. Detailed information and preparation of the two chelating agent used in this study are summarized below:

Ethylenediamine tetra-acetic acid (EDTA): is one of the most common chelating agents used in chemistry. The aqueous form of EDTA is a clear to slightly yellow solution prepared by dissolving $Na_2EDTA2H2O$ salt in deionized water with NaOH. The EDTA solution used here was purchased from Fisher Science at its maximum solubility (~10g/100mL water at room temperature) with pH adjusted to 12 and injected as pretreatment undiluted.

Sodium triphosphate (STP): is another widely used chelating agent. In this study, STP solution was prepared by dissolving white crystal $Na_5P_3O_{10}$ in DI water at its maximum solubility (14.5g/100mL water at room temperature). The prepared STP solution was mostly used for pretreatment before polymer injection; however, it was also tested as an additive in the polymer dispersion. In addition, it is strongly advised that this procedure be done under a well-ventilated fume hood due to the toxicity of STP at high concentrations.

1.2.2 Core preparation

Core samples were created using class H neat cement cured in sealed molds for four days at 100 °F and atmospheric pressure. Three types of fracture surfaces are created using the following methods:

Cement-cement core. Cylindrical cement core (1" diameter × 6" length) cured in a thin plastic tube was removed and sawed in half using a rock saw. The cement half is shown in **Fig. 8(a)** has blade marks on the sawed surface that can provide a semi-smooth flow path and a small offset when two halves are re-constructed.

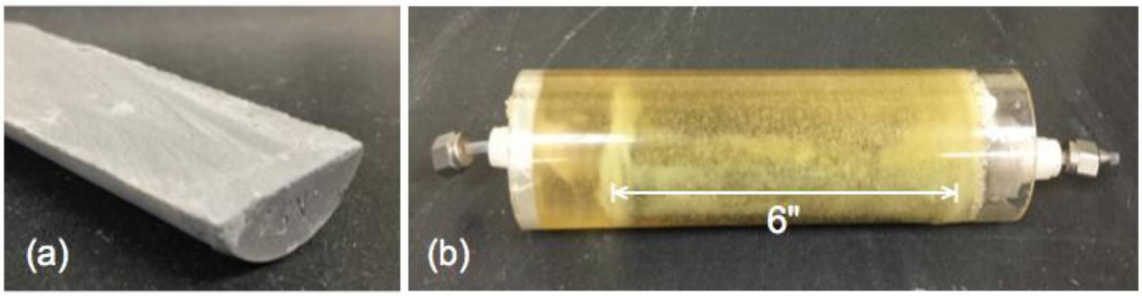

Fig. 8 – Cement-cement core preparation and construction (a) rough sawed cement surface, and (b) two halves epoxied in a polycarbonate tube with ends connected.

Two sawed cement surfaces were placed against each other and placed inside a polycarbonate tube filled with epoxy. The double-surface cement pathway was sealed inside the tube with ends connected to inlet/outlet for injection as seen in **Fig. 8(b)**. This type of core allows double cement surface area to be in contact with polymer dispersion mimicking the actual cement fracture at the wellbore (Patterson 2014).

Cement-plastic core. Smooth-surface cement cores (10" or 6" length × 1" width) were created using a mold made with thin plastic sheets cut to two specific dimensions (1"×1" and 1"×10") and constructed to form a rectangular prism with one 1"×10" side left open as illustrated in **Fig. 9(a)**. Cement slurry was poured then cured in the mold and held together by waterproof duct tape; thus a smooth surface could be created upon removal from the mold as seen in **Fig. 9(a)**.

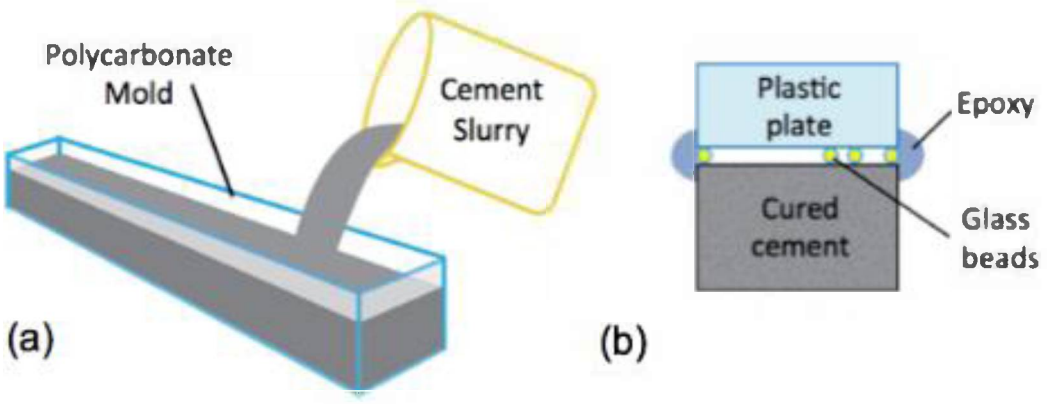

Fig. 9 – Illustrations of (a) plastic mold and (b) the construction of the cement-plastic plate core.

To construct the flow path, a smooth cement surface was placed against a transparent plastic plate with glass beads of known diameter (100-1,000 microns) placed between as spacers in attempt to create the desired fracture aperture [**Fig. 9(b)**]. The fracture created by the cement and plastic plate was then sealed with epoxy around the fracture edges and cement while the front of the transparent plastic plate was left un-epoxied to allow visual inspection of reactions in the fracture (**Fig. 10**). The cement-plastic construction would allow a homogeneous reaction between one cement surface with the polymer dispersion and simplifies the fracture geometry to aid reactive transport simulations.

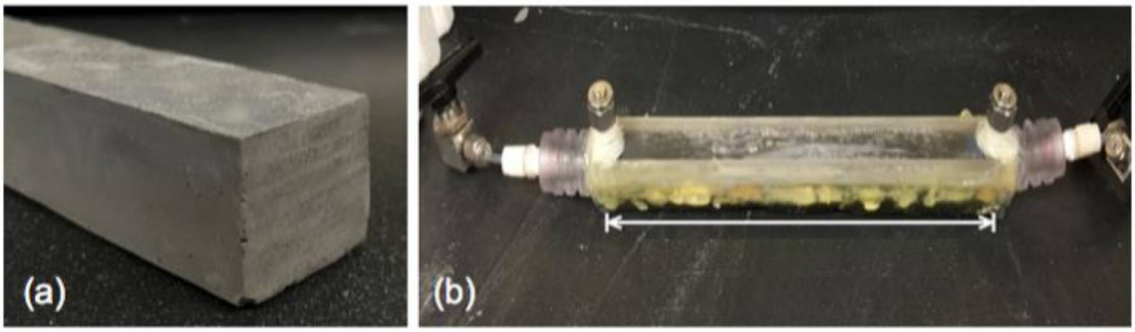

Fig. 10 – Cement-plastic core preparation and construction (a) smooth cement surface with glass beads, and (b) 6" or 10"-length cement with smooth surface placed against a polycarbonate plastic plate with back and sides epoxied.

Fractured Cement in Hassler coreholder. The Brazilian fracturing method used in this study originated from the Brazilian test that is commonly used to determine the tensile strength of rocks (Guo et al. 1993). In the Brazilian test, most cylindrical rock specimens fail in tension, along the length of the core, when subjected to sufficient compressive loads. The same fracturing method is used for the cement in attempt to create a tensile fracture mimicking naturally formed fractures. The cylindrical cement core is placed laterally in a rock compressor consisting of two disc-shaped load frames, and is then subjected to a compressive load large enough to fracture the cement.

Cement cores with diameter greater than 1" typically fractures the core into two halves forming an irregular tensile fracture along the length of the core as seen in **Fig. 11(a)**. Despite previous

successes using the method for cores with larger diameters, all 7/8" cores shattered to pieces and failed to create a tensile fracture along the length of the cores [**Fig. 11(b)**]. There seems to be a lower limit in core diameter for which the method could be used.

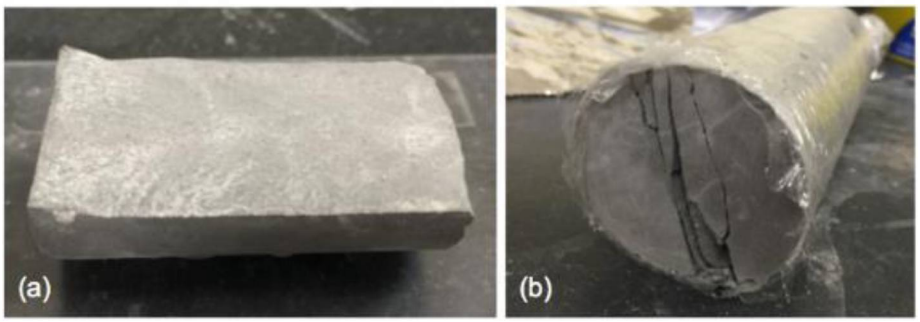

Fig. 11 – The Brazilian fracturing method (a) irregular tensile fracture, and (b) shattered cement core held together by the plastic wrap.

1.2.3 Experimental procedure and setup

In this section, we explain the experimental procedure and setup for fracture permeability tests, pretreatment and polymer placement, and gel strength testing.

1.2.3.1 Fracture permeability test

Sealed cement core is placed under the vacuum pump for at least 12 hours, then saturated with deionized (DI) water for at least 24 hours. A standard permeability test with the injection of DI water is performed at various flow rates while measuring pressure drop in order to determine the effective hydraulic aperture of the slit, B ("effective" because the slit's aperture changes along the length and width of the core),

$$B = \left(\frac{12\mu QL}{W\Delta P}\right)^{1/3}, \tag{2}$$

where μ is water viscosity, Q is volumetric flow rate, L is the length and W is the width of the fracture, and ΔP is the pressure drop across the length of the fracture (all units in SI). During DI water injection into the cement fractures, the flow rates of 200, 160, 100, 20 mL/min are set by the pump while inlet and outlet pressures are recorded by a differential pressure transducer. The pressure drops for the different flow rates are averaged and the hydraulic aperture is calculated for each flow rate. These hydraulic apertures are then averaged to obtain the estimated average hydraulic aperture, B. An example of the pressure response during a permeability test is shown below in **Fig. 12**, with which the average aperture calculated from the four flow rates was 0.489

mm. This aperture can be used to determine the volume of the fracture and the apparent viscosity of the polymer during injection.

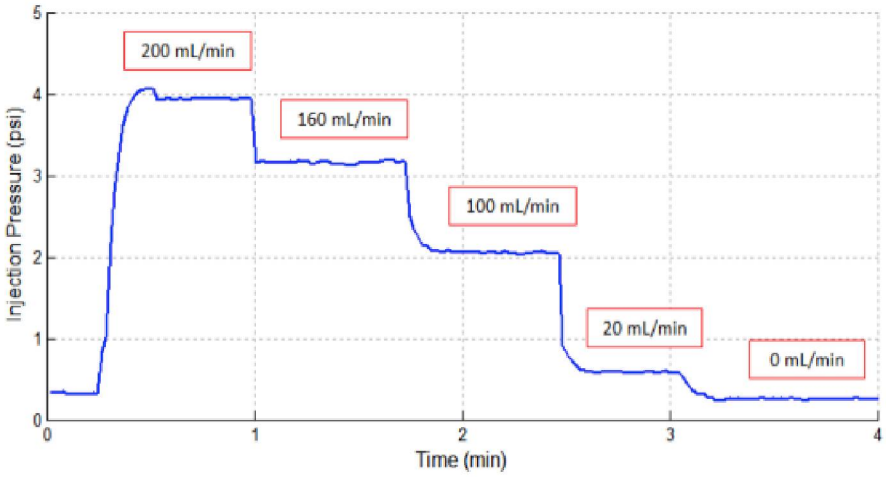

Fig. 12 – Standard permeability tests are performed to estimate the fracture hydraulic aperture (Patterson 2014).

1.2.3.2 Pretreatment and polymer placement

Although some experiments were carried out using syneresis inhibitors as additives in the polymer solution during polymer injection, the majority of experiments were conducted using separate pretreatment stage for cement fractures prior to polymer injection. Because most syneresis inhibitors are very alkaline, it prematurely increases the pH and viscosity/yield stress of the polymer when used as additives; thereby injection into cement fractures may be difficult.

Cement pretreatment is performed by injecting syneresis inhibitors into the fracture volume and allowing time for chemicals to react with calcium ions leaching out from fracture surfaces. The calcium is captured in the reacted chemical then removed by polymer displacement. In some cases, it may be necessary to use DI water to flush out the pretreatment solution before polymer injection to prevent premature gelling. **Fig. 13** is an illustration of the pretreatment setup where two Chromaflex glass columns are used to hold and inject fluids. The purpose of placing a volume of mineral oil in between chemical and water from the pump is to prevent mixing as water displaces oil and drive chemicals into the core. In this study, most cores were pretreated with syneresis inhibitors for durations between 10 minutes to 24 hours before polymer injections.

When polymer injection is performed, the glass columns must be replaced with a steel accumulator that is resistant to pressurized fluids. Pressure drop during polymer injection was recorded for some of the cores, to better characterize reactions in the fracture during injection and to determine polymer injectivity. For most other samples, one fracture volume of 3 wt% Carbopol 934 (dyed blue) was injected and shut for various periods of time to allow gel development.

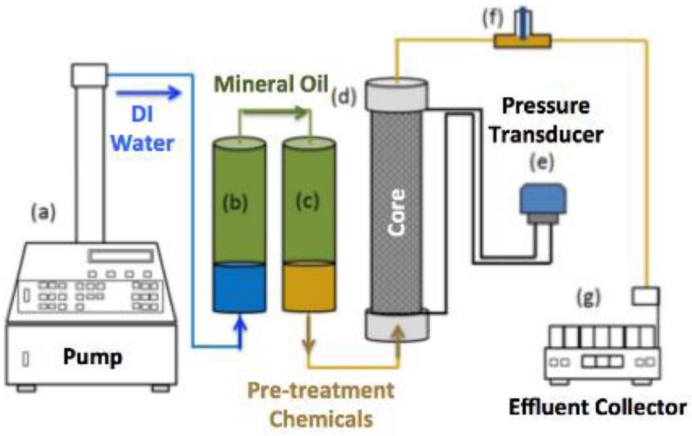

Fig. 13 – The experimental setup for pretreatment of the cement core sample. (a) ISCO Syringe Pump, (b) Chromaflex glass column of oil (green) above DI water (blue), (c) Chromaflex glass column of oil (green) above pretreatment solution (orange), (d) cement core sample, (e) differential pressure transducer, (f) pH probe, and (g) effluent collector. The polymer injection experiments are done under similar experimental set up by replacing (b) and (c) with a steel accumulator. In the accumulator, DI water is placed on one side of the piston and polymer dispersion is placed on the other side (Patterson 2014).

1.2.3.3 Gel strength testing

In this section, we provide the experimental procedure and setup for gel strength testing using water and CO_2 breakthrough tests.

1.2.3.3.1 Water breakthrough test

After the polymer placement and shut-in for different periods of time, water breakthrough tests were performed to obtain holdback pressure over the length of the cores. The test is used to determine the strength of the reacted gel that is formed in cement fracture samples. Both DI water and acidic brine are used as the holdback fluid to test the effect of an acidic environment on gel strength. During the test, pressure drop is increased gradually by pumping the holdback test fluid at a very slow rate (0.25 mL/min) to minimize the disturbance of the reacted gel structure in the fracture in order to mimic an instantaneous constant pressure applied against the placed gel. The maximum pressure drop before liquid breakthrough is recorded as the maximum holdback pressure and the holdback pressure gradient (psi/ft) was calculated based on the length of the core (either 6" or 10"). Thus, the gel in place is expected to hold back any constant pressure below the maximum holdback pressure. **Fig. 14** is the representation of a typical liquid breakthrough test. As this figure shows the pressure increases steadily until the maximum holdback pressure is reached and pressure drops drastically after the water is broken through the gel.

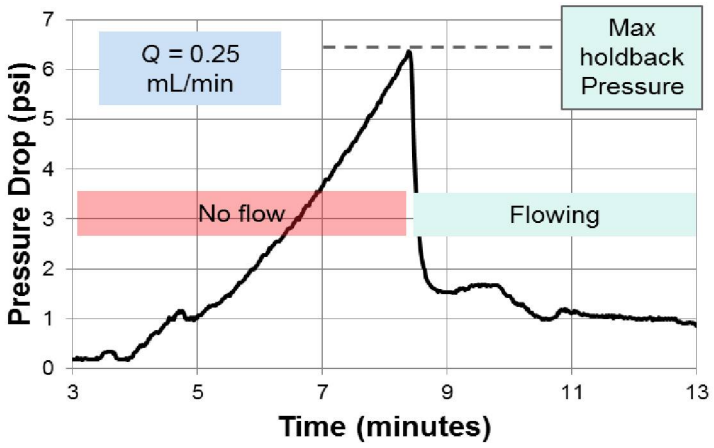

Fig. 14 – An example of gel resistance to pressure buildup in a standard liquid breakthrough test. The test is used to determine the strength of the reacted gel that was placed in the fracture. The holdback pressure gradient is a representation of the gel strength and can be compared to pressure gradients in existing leaky wellbore conditions (Patterson 2014).

The holdback pressure gradients of the gel were then compared with the theoretical pressure gradients calculated from the gel yield stress measured in polymer rheology experiments. Theoretical pressure gradients can be calculated as

$$\left(\frac{\Delta P}{\Delta L}\right)_{theoretical} = \frac{2\sigma_y}{r_H} \quad , \tag{3}$$

where σ_y is the polymer-gel yield stress (psi) and r_H is the hydraulic radius of the aperture calculated as

$$r_H = \frac{WB}{2(W+B)} \quad , \tag{4}$$

where W is the core width and B is the effective fracture aperture. In addition to the aforementioned gel strength tests using water injection, the gel strength tests with injection of acidic brine, and also with CO_2 gas plume, were conducted. Several liquid breakthrough tests were done by injecting acidic brine that was made by adding HCl into 2 wt% NaCl until pH=2 was reached. A flow chart of the standard procedure performed in this study is illustrated in **Fig. 15**. The exact details may be slightly different for individual experiments; the procedures are more or less the same.

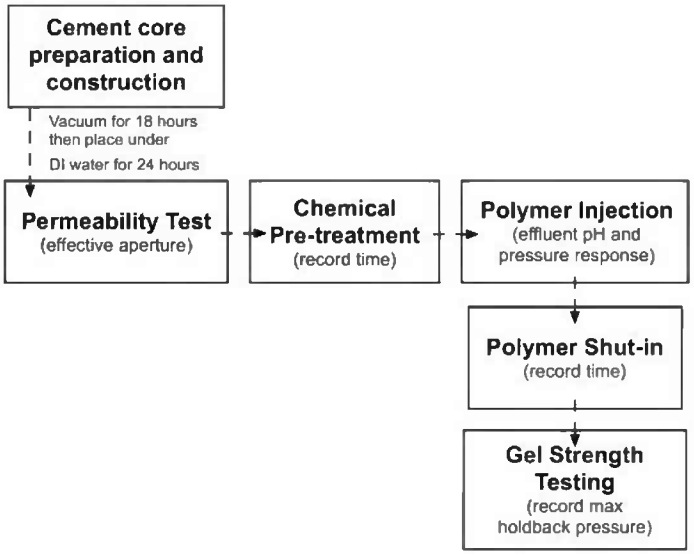

Fig. 15 – Flow chart of standard experimental procedure performed in this study.

1.2.3.3.2 CO_2 breakthrough test

The CO_2 breakthrough test is discussed here. The core preparation is elaborated first and tests using low and high pressure CO_2 are discussed next.

1.2.3.3.2.1 Core Preparation

The 7/8" and 1 7/8" diameters were chosen for the cement core in consideration for the thickness of heatshrink wrapping before fitting into the Hassler coreholders. Heatshrink wrapping is a precautionary procedure as to prevent chemicals or CO_2 from damaging the hydraulic rubber sleeve inside the coreholder. 7/8" diameter × 6" length cylindrical cores are cored from a cured cement block (6"×6"×8") and wrapped tightly with one layer of Teflon tape. The wrapped core is then fractured into pieces using the Brazilian method, as previously mentioned, with Teflon wrapping keeping the pieces intact. The resulting cement fracture is not a single tensile fracture and its fracture geometry is unknown. 1 7/8" diameter × 6" length cylindrical cores are cored from the cured cement block and sawed in half with a rock saw. **Table 1** lists the dimensions and details of the cement cores used in our experiments.

Table 1 – Dimensions and detail of the cement cores prepared for CO_2 breakthrough tests. Heatshrink wraps were purchased from Geophysical Supply Company (Houston, Texas).

Pressure Holdback Test	Cement Core Dimension (diameter x length)	Coreholder Dimension (diameter x length)	Fracture Method	Heatshrink Wrapping (diameter)
Low Pressure CO2	7/8" x 6"	1" x 1'	Brazilian	1.5"
High Pressure CO2	7/8" x 6"	1" x 1'	Brazilian	1.5"
High Pressure CO2	1 7/8" x 6	2" x 1'	Sawed	2"

A 6" steel spacer is placed before the 6" Teflon wrapped core to extend the total length to 1 ft. Two end connections from the coreholder are placed at both ends of the extended core, then slid into a 1.5" heatshrink wrap tube with length sufficient to wrap at least ½" of each end connections. It is necessary to have heatshrink wrap longer than the length of the inserted core to effectively prevent chemicals or CO_2 from contacting the rubber sleeve inside the coreholder. The entire construction is then placed in an oven set at 50°C for 10-15 minutes until it can be held tightly by the heatshrink. The construction with enclosed fractured cement is loaded into the Hassler coreholder, then vacuumed and soaked with DI water under a confining pressure. The Hassler coreholders used in this study were manufactured by Pheonix Instruments with different dimensions and pressure limits as seen in **Fig. 16**.

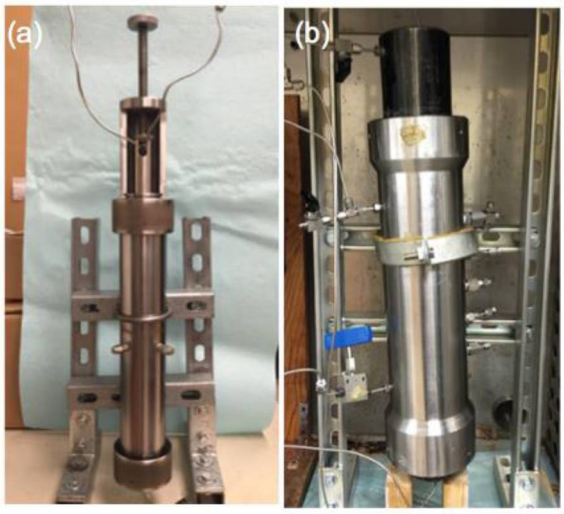

Fig. 16 – Specifications of the 12"-long steel coreholders manufactured by Pheonix Instruments (a) 1" diameter Hassler coreholder (working pressure: 1,250 psi), and (b) 2" diameter Hassler coreholder (working pressure: 5,000 psi).

The main advantage of using the Hassler coreholder is that tests can be performed at higher pressures (> 100 psi) and remain sealed for longer durations without premature termination due to core material failure. In case of a leak in the wrapped core, selection of the hydraulic rubber sleeve depends on the fluid used in the experiment: Viton tubing is resistant to chemical and most hydrocarbon exposure, while Aflas is good for CO_2 exposure.

1.2.3.3.2.2 Low-pressure CO_2 test

A preliminary CO_2 holdback test was carried out in low-pressure setting (under 100 psi) to determine if gel would be weakened when placed in contact with pressurized CO_2 gas for an extended time. The experiment was done in the Hassler coreholder with a fractured 7/8"×6" cylindrical cement. A confining pressure set at 100 psi was used throughout the procedures. **Fig. 17** is the experimental setup. The Hassler coreholder was connected to the CO_2 cylinder (full tank at 800 psia) through two pressure regulators to step down the pressure. During the test, the pressure transducer measured and recorded the pressure drop across the length of the core. When the reacted gel in the fractured cement sample was broken through, the pressure drop is expected to drop and the CO_2 will bubble through the outlet, which will be seen in the beaker filled with water. The inlet pressure was initially set at 5 psi and increased by 5 psi over the course of 30 minutes until the maximum gauge pressure was reached at 30 psi and left to holdback this constant pressure for two weeks until a second breakthrough test was done with pH=4 acidic brine (2 wt% NaCl).

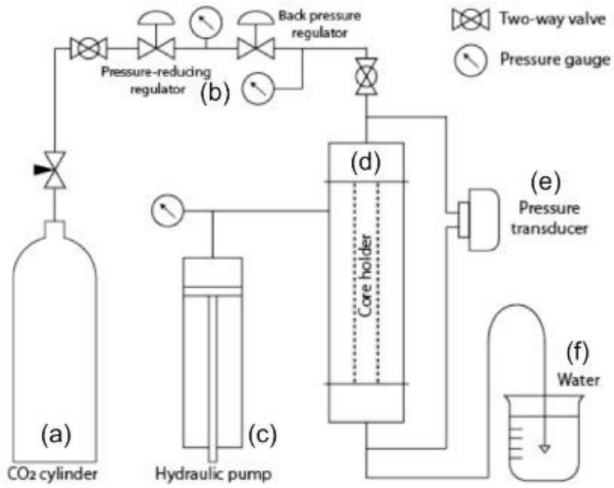

Fig. 17 – The experimental setup for low-pressure CO_2 breakthrough test done at standard conditions: (a) CO_2 cylinder tank (CO_2 > 99% purity) from Matheson Tri-Gas Inc. (Basking Ridge, NJ), (b) pressure-reducing and back-pressure regulators from Swagelok Inc., (c) Enerpac P-392 hydraulic hand pump, (d) 1" Hassler coreholder, (e) Rosemount pressure transducers, and (f) beaker filled with water (Ho et al. 2015).

1.2.3.3.2.3 High-pressure CO_2 test

Two high-pressure CO_2 tests were performed to determine polymer gel's resistance to supercritical CO_2 to mimic geological storage conditions. CO_2 can be compressed to reach the supercritical state when both temperature and pressure equal or exceed its critical point of 31°C and 1,073 psi.

Fig. 18 illustrates the experimental setup for the supercritical CO_2 holdback test. The coreholder was placed in an oven set at 70°C with inlet connected to the CO_2 accumulator and outlet connected to a back-pressure regulator (BPR). The BPR is pre-set at 1,100 psi prior to the start of the experiment to ensure pressure in the coreholder remains above the supercritical state unless core is broken through. Pressure transducers connected to the inlet and outlet of the coreholder measures the pressure buildup during the holdback and detects pressure drop when CO_2 breaks through.

Once pressure in the CO_2 accumulator reaches above 1,100 psi, the supercritical CO_2 is let into the core and pressure starts to build up as the HPLC pump continues to pump the supercritical CO_2. Once the gel is broken through, effluent CO_2 is cooled down by flowing in the coiled outlet line submerged in a hot water bath set at 70°C to prevent freezing caused by the dramatic pressure decrease. Effluent is then redirected to a fume hood.

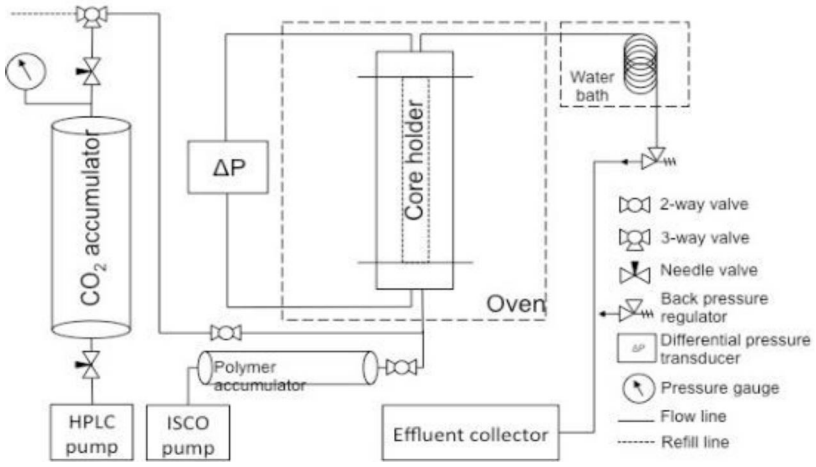

Fig. 18 – Supercritical CO_2 holdback test setup. The fractured cement core is placed into the Hassler coreholder under a fixed temperature in the oven (a). The ISCO pump (b) can be used to pump the pretreatment fluid and polymer dispersion pre-filled in an accumulator (c). After the polymer placement and shut-in for a period of time to develop yield stress, a separate line can be used to inject the supercritical CO_2 from the floating-piston accumulator (d) pressurized by a HPLC dual piston pump (e). Various reasonable pressure gradients will be set across the core with the use of the back-pressure regulator (f) and the pressure transducers (g). The effluent supercritical CO_2 will pass through a heated water bath (h) to prevent the CO_2 from freezing the tubings caused by the sudden pressure drop. Cooled CO_2 effluent is then collected through the effluent collector (i) and redirected to a fume hood.

1.3 CEMENT ANNULUS BENCH TEST

The setup is analogous to a real cement wellbore in a shallow formation. The cement annulus is created using two pipes that differ in diameter; where the smaller inner pipe mimicking a steel casing, and the larger pipe mimicking an openhole condition in an impermeable formation. Manmade-fractures are created inside the annulus to mimic leakage pathways where the polymer could be inserted and gel strength could be tested under ambient conditions.

1.3.1 Preparation and experimental setup

Two pipes are used to create a cement annulus: the small 1" inner pipe and the large 2.5" outer pipe (with the bottom sealed by a cap). First, a removable PVC cap is used to cap the bottom of the large pipe and 2" of sand is placed at the bottom section. Second, a slightly longer inner pipe is placed in the middle of the larger pipe and pushed down into the bottom sand. Cement slurry is then poured in slow circular motion into the annulus space to minimize air pockets that can form in the cement annulus; with one inch length from the top of the annulus left unfilled.

To create a long vertical channel, a straightened 1.5 mm metal wired is greased and inserted into the cement annulus. The cement is then left undisturbed for 24 hours before the greased wire is pulled out. The bottom cap is removed and sand is cleaned out. Finally, the removable cap is glued to the bottom with PVC glue. **Fig. 19** is an illustration of the construction. To make the fractured cement annulus, another bench test was performed using the same method but using a flexible Tygon tubing as the outer pipe. The cement annulus is set for 24 hours without inserting a wire. The random fractures were later created by hammering the outer Tygon tubing.

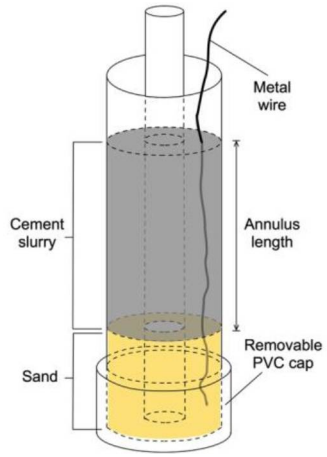

Fig. 19 – Cement annulus bench test construction and setup. The bottom of the larger pipe is capped with a PVC cap. Sand is placed in the pipe at the bottom with the inner tube pushed into the sand. Cement slurry is poured into the annulus space and a metal wire is inserted all the way to the bottom of the cement to create a leakage channel. After the cement sets, the bottom cap and wire are removed and sand is cleaned out. Finally, the PVC cap is glued to the bottom of the large pipe ready for chemical pretreatment and polymer injection.

1.3.2 Experimental procedure

Both types of cement annulus bench tests are pretreated with sodium triphosphate for 24 hours, then injected with polymer until polymer immerges from the top of the annulus. Subsequently, the top of the annulus is added with some water and sealed up with parafilm to prevent dehydration. The injected polymer in cement annulus is left to shut-in for more than 24 hours. After polymer shut-in, top of the hollow inner tubing is connected to compressed air so that a constant pressure can be applied to the bottom of the sealed annulus as seen in **Fig. 20**. The constant pressure applied is set according to a reasonable static holdback pressure gradient of around 15 psi/ft. This constant pressure gradient is monitored for one week before moving on to higher pressure gradients for testing the maximum holdback pressure for breakthrough.

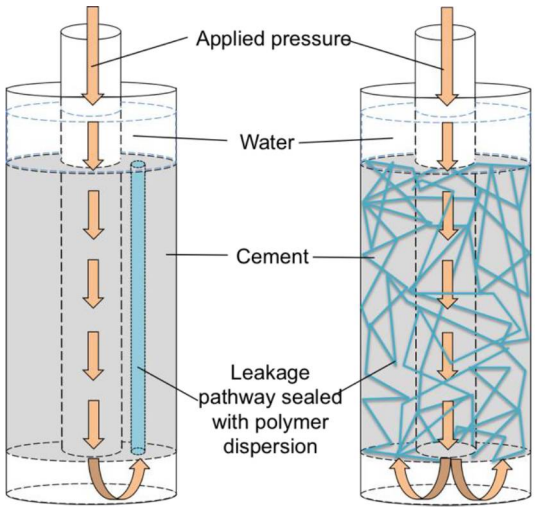

Fig. 20– Cement annulus bench test with channel pathway PVC-1 (left) and fractured pathway TYG-1 (right), then applied with a constant pressure at the bottom by hooking the top of the inner pipe to stream of compressed air for a period of time. If the seal held over time, a gel strength testing at higher pressures can be done with the increase of the compressed air pressure until the gel is broken through.

1.4 MODELING

Modeling can be used to better understand and predict the process. The primary step is to understand the underlying mechanisms for modeling. This task was done on the basis of the profound understanding of the process based on the extensive experimental study and by constructing the sets of equations and relevant initial and boundary conditions (Tavassoli et al. 2016). The equations include flow equations of microgel (polymer gel), transport equations of species, and auxiliary equations. These equations are explained in details in the following paragraphs.

1.4.1 Model development

The flow of the microgel in the fracture can be captured by a slit-flow model (Tavassoli et al. 2016). **Fig. 21** illustrates a simplified version of this model for the half of the slit below the centerline. The polymer at a low pH (about 2.5) is injected at the inlet. The microgel apparent viscosity increases as soon as it contacts the cement surface as a result of an increase in the pH. The polymer has shown non-Newtonian behavior. Hence, polymer rheology should be captured on the basis of the non-Newtonian behavior studied in the experiments and transport properties of proton (H^+) or hydroxide (OH^-) and polymer solutes. Diffusive properties of these species are required to model the transport along the fracture and from the wall towards the centerline (perpendicular).

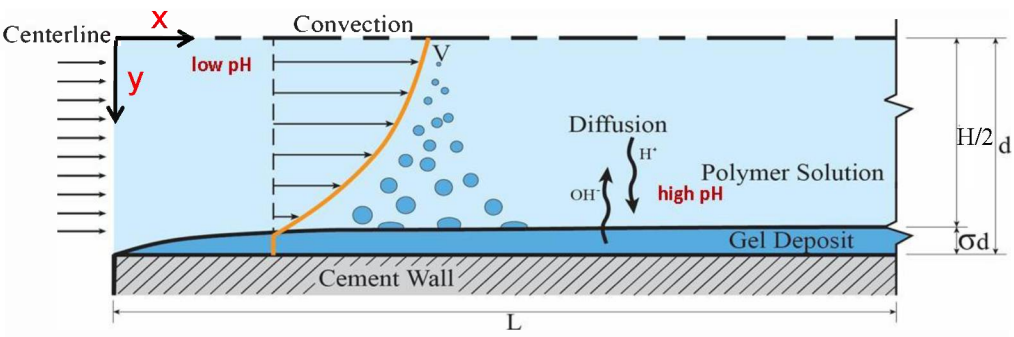

Fig. 21 – Illustration of the flow and boundary geometry.

Fig. 22 shows the geometry of the slit representative of the cement fracture. Microgel is being injected at the inlet of the slit. The mesh grids generated by COMSOL Multiphysics (2015) for solving this problem is also shown in this figure. The simulation results were obtained using COMSOL Multiphysics (2015) to solve the underlying equations.

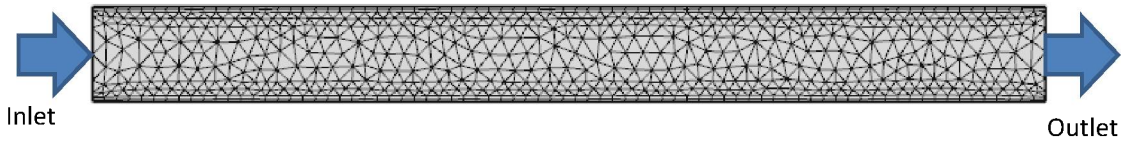

Fig. 22 – Illustration of the slit geometry representative of the cement fracture.

Fig. 23 shows the calculation flow chart for the modeling of the process. The first step is to make sure that our rheology model is consistent with the rheology data measured in the lab. The polymer rheology behavior is dependent on shear rate, polymer concentration, pH, and salinity. Hence, it is very important to develop a model based on the polymer rheology measurements that captures the polymer behavior and effects of reactive solutes. The second step is to model the transport properties based on our flow tests. In case of an unacceptable match, we can calibrate the transport model and/or kinetic and rheology parameters.

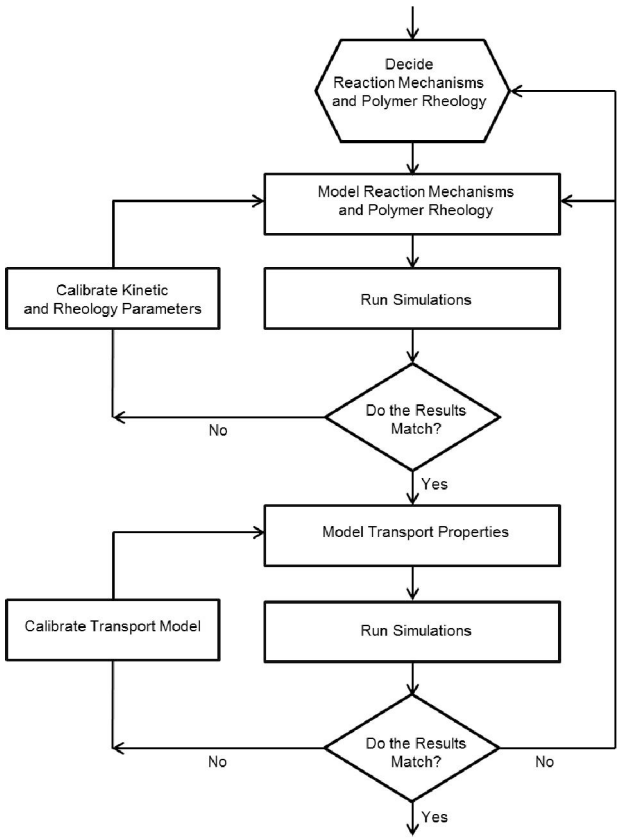

Fig. 23 – Simulation Flow Chart.

1.4.2 Mathematical formulation

In this section, we provide the governing equations. The underlying equations and initial and boundary conditions were further non-dimensionalized to better understand the significance of various physical effects and to facilitate the scaleup to larger scales.

1.4.2.1 Flow equations

The single-phase fluid flow can be modeled based on the Navier-Stokes equations as follows:

$$\frac{\partial \rho}{\partial t} + \nabla \cdot (\rho \boldsymbol{u}) = 0\,, \tag{5}$$

$$\rho \frac{\partial \boldsymbol{u}}{\partial t} + \rho(\boldsymbol{u} \cdot \nabla)\boldsymbol{u} = \nabla \cdot \left[-P\mathbf{I} + \tau\right] + \mathbf{F}\,, \tag{6}$$

Inserting the equation for τ in Eq. 6 results in:

$$\rho \frac{\partial \boldsymbol{u}}{\partial t} + \rho(\boldsymbol{u} \cdot \nabla)\boldsymbol{u} = \nabla \cdot \left[-P\mathbf{I} + \mu(\nabla \boldsymbol{u} + (\nabla \boldsymbol{u})^T) - \frac{2}{3}\mu(\nabla \cdot \boldsymbol{u})\mathbf{I} \right] + \mathbf{F}\ , \tag{7}$$

where ρ is density (kg/m^3), $\boldsymbol{u}$ is velocity vector (m/s), P is pressure (Pa), τ is viscous stress tensor (Pa), and **F** is volume force vector (N/m^3). Eqs. 5 and 7 can be simplified as follows:

$$\nabla \cdot \mathbf{u} = 0 \ , \tag{8}$$

$$\rho \frac{\partial \boldsymbol{u}}{\partial t} = \mu \nabla^2 \mathbf{u} - \nabla p \ , \tag{9}$$

Initial and boundary conditions are as follows:

$$\boldsymbol{u} = \boldsymbol{u}_{in} \,@\, x = 0; \ \ p = p_{out} \,@\, x = L$$
$$u_y = 0 @ y = H; \ \ \frac{\partial u_y}{\partial y} = 0 @ y = 0$$
$$u_x = u_y = 0 @ t = 0$$

1.4.2.2 Transport equations

The transport of chemical species through diffusion and convection using the mass balance can be written as follows:

$$\frac{\partial c}{\partial t} + \boldsymbol{u} \cdot \nabla c = \nabla \cdot \left(D \nabla c \right) + R \ , \tag{10}$$

where c is concentration of species (mol/m^3), D is diffusion coefficient (m^2/s), R is reaction rate [mol/(m^3.s)], and $\boldsymbol{u}$ is velocity vector (m/s). The following equations can be written for concentration of polymer, proton (H^+), and hydroxide (OH^-):

$$\frac{\partial c_p}{\partial t} = \frac{\partial}{\partial x}\left(D_x \frac{\partial c_p}{\partial x} \right) + \frac{\partial}{\partial y}\left(D_y \frac{\partial c_p}{\partial y} \right) - u_x \frac{\partial c_p}{\partial x} - u_y \frac{\partial c_p}{\partial y} \ , \tag{11}$$

$$\frac{\partial c_{H^+}}{\partial t} = \frac{\partial}{\partial x}\left(D_x \frac{\partial c_{H^+}}{\partial x} \right) + \frac{\partial}{\partial y}\left(D_y \frac{\partial c_{H^+}}{\partial y} \right) - u_x \frac{\partial c_{H^+}}{\partial x} - u_y \frac{\partial c_{H^+}}{\partial y} + r_{H^+} \ , \tag{12}$$

$$\frac{\partial c_{OH^-}}{\partial t} = \frac{\partial}{\partial x}\left(D_x \frac{\partial c_{OH^-}}{\partial x} \right) + \frac{\partial}{\partial y}\left(D_y \frac{\partial c_{OH^-}}{\partial y} \right) - u_x \frac{\partial c_{OH^-}}{\partial x} - u_y \frac{\partial c_{OH^-}}{\partial y} + r_{OH^-} \ , \tag{13}$$

Initial and boundary conditions are as follows:

$$c_p = c_{in} @ x = 0; \quad \frac{\partial c_p}{\partial x} = 0 @ x = L$$

$$c_{H^+} = 0 @ y = H; \quad \frac{\partial c_{H^+}}{\partial y} = 0 @ y = 0$$

$$c_{OH^-} = 1 @ y = H; \quad \frac{\partial c_{OH^-}}{\partial y} = 0 @ y = 0$$

$$c_p = c_{in} @ t = 0$$

$$c_{H^+} = 10^{-pH_{inlet}} @ t = 0$$

$$c_{OH^-} = 10^{-(14-pH_{inlet})} @ t = 0$$

1.4.2.3 Dimensionless form of flow equations

Flow equations (Eqs. 8 and 9) can be written in two dimensional coordinates as follows:

$$\frac{\partial u_x}{\partial x} + \frac{\partial u_y}{\partial y} = 0 \ , \tag{14}$$

$$\rho(\frac{\partial u_x}{\partial t}) = \mu(\frac{\partial^2 u_x}{\partial x^2} + \frac{\partial^2 u_x}{\partial y^2}) - \frac{\partial p}{\partial x} \ , \tag{15}$$

$$\rho(\frac{\partial u_y}{\partial t}) = \mu(\frac{\partial^2 u_y}{\partial x^2} + \frac{\partial^2 u_y}{\partial y^2}) \ . \tag{16}$$

The initial and boundary conditions are as follows:

$$u_x = u_{x,in} @ x = 0; \ u_y = u_{y,in} @ x = 0$$

$$p = p_{out} @ x = L$$

$$u_y = 0 @ y = H; \quad \frac{\partial u_y}{\partial y} = 0 @ y = 0$$

$$u_x = u_y = 0 @ t = 0$$

By introducing the following dimensionless groups:

$$u_{D,x} = \frac{u_x}{u_{0,x}}, \ x_D = \frac{x}{L} \ , \quad y_D = \frac{y}{H} \ , \ t_D = t_{D,x} = \frac{u_x t}{L} \ , \ t_{D,y} = \frac{u_y t}{H}$$

$$P_D = \frac{P - P_{out}}{\mu u_{0,x} / L} \ , \ R_L = \frac{L}{H} , \ Re_x = \frac{\rho H u_x}{\mu} , \ Re_y = \frac{\rho L u_y}{\mu}$$

Eqs. 14 through 16 can be written in the dimensionless form as follows:

$$\frac{\partial u_{D,x}}{\partial x_D} + \frac{t_{D,x}}{t_{D,y}} \frac{\partial u_{D,y}}{\partial y_D} = 0 , \tag{17}$$

$$\frac{\partial u_{D,x}}{\partial t_D} = \frac{1}{R_L Re_x} \left(\frac{\partial^2 u_{D,x}}{\partial x_D^2} + R_L^2 \frac{\partial^2 u_{D,x}}{\partial y_D^2} - \frac{\partial p_D}{\partial x_D} \right) , \tag{18}$$

$$\frac{\partial u_{D,y}}{\partial t_{D,y}} = \frac{R_L}{Re_y} \left(\frac{1}{R_L^2} \frac{\partial^2 u_{D,y}}{\partial x_D^2} + \frac{\partial^2 u_{D,y}}{\partial y_D^2} \right) . \tag{19}$$

The initial and boundary conditions in dimensionless form as follows:

$$\boldsymbol{u}_0 = \boldsymbol{u}_{\boldsymbol{in}} = (u_{0,x}, u_{0,y})$$

$$u_{D,x} = 1 @ x_D = 0; \ u_{D,y} = 1 @ x_D = 0$$
$$p_D = 0 @ x_D = 1$$
$$u_{D,y} = 0 @ y_D = 1; \ \frac{\partial u_{D,y}}{\partial y_D} = 0 @ y_D = 0$$
$$u_{D,x} = u_{D,y} = 0 @ t_D = 0$$

1.4.2.4 Dimensionless form of transport equations

Transport equation (Eq. 10) can be written in two dimensional coordinates as follows:

$$\frac{\partial c}{\partial t} + u_x \left(\frac{\partial c}{\partial x} \right) + u_y \left(\frac{\partial c}{\partial y} \right) - D_x \left(\frac{\partial^2 c}{\partial x^2} \right) - D_y \left(\frac{\partial^2 c}{\partial y^2} \right) = k(c_0 - c) , \tag{20}$$

By introducing the following dimensionless groups:

$$x_D = \frac{x}{L} \ , \ y_D = \frac{y}{H} \ , \ c_D = \frac{c}{c_0} \ , \ t_D = t_{D,x} = \frac{u_x t}{L} \ , \ t_{D,y} = \frac{u_y t}{H}$$

$$R_L = \frac{L}{H} , \ Pe_x = \frac{u_x L}{D_x} \ , \ Pe_y = \frac{u_x H^2}{D_y L} \ , \ Da = \frac{kL}{u_x}$$

Eq. 20 can be written in non-dimensional form:

$$\frac{\partial c_D}{\partial t_D}+\frac{\partial c_D}{\partial x_D}+{t_{D,y}}\Big/{t_{D,x}}\,\frac{\partial c_D}{\partial y_D}-{1}\Big/{Pe_x}\,\frac{\partial^2 c_D}{\partial x_D^2}-{1}\Big/{Pe_y}\,\frac{\partial^2 c_D}{\partial y_D^2}=Da(1-c_D)\ , \tag{21}$$

Initial concentrations for polymer, proton (H^+), and hydroxide (OH^-) are as follows:

$$c_{0,p}=c_{in}$$
$$c_{0,H^+}=10^{-pH_{inlet}}$$
$$c_{0,OH^-}=10^{-(14-pH_{inlet})}$$

Hence, Eqs. 11-13 can be written in non-dimensional form as

$$\frac{\partial c_{D,p}}{\partial t_D}={1}\Big/{Pe_{x,P}}\,\frac{\partial^2 c_{D,P}}{\partial x_D^2}+{1}\Big/{Pe_{y,P}}\,\frac{\partial^2 c_{D,P}}{\partial y_D^2}-\frac{\partial c_{D,P}}{\partial x_D}-{t_{D,y}}\Big/{t_{D,x}}\,\frac{\partial c_{D,P}}{\partial y_D}\ , \tag{22}$$

$$\frac{\partial c_{D,H^+}}{\partial t}={1}\Big/{Pe_{x,H^+}}\,\frac{\partial^2 c_{D,H^+}}{\partial x_D^2}+{1}\Big/{Pe_{y,H^+}}\,\frac{\partial^2 c_{D,H^+}}{\partial y_D^2}-\frac{\partial c_{D,H^+}}{\partial x_D}-{t_{D,y}}\Big/{t_{D,x}}\,\frac{\partial c_{D,H^+}}{\partial y_D}+Da_{H^+}(1-c_{D,H^+})\,, \tag{23}$$

$$\frac{\partial c_{D,OH^-}}{\partial t}={1}\Big/{Pe_{x,OH^-}}\,\frac{\partial^2 c_{D,OH^-}}{\partial x_D^2}+{1}\Big/{Pe_{y,OH^-}}\,\frac{\partial^2 c_{D,OH^-}}{\partial y_D^2}-\frac{\partial c_{D,OH^-}}{\partial x_D}-{t_{D,y}}\Big/{t_{D,x}}\,\frac{\partial c_{D,OH^-}}{\partial y_D}+Da_{OH^-}(1-c_{D,OH^-})\,, \tag{24}$$

The initial and boundary conditions are as follows:

$$c_{D,p}=1@\,x_D=0;\quad \frac{\partial c_{D,p}}{\partial x_D}=0@\,x_D=1$$
$$c_{D,H^+}=0@\,y_D=1;\quad \frac{\partial c_{D,H^+}}{\partial y_D}=0@\,y_D=0$$
$$c_{D,OH^-}=1@\,y_D=1;\quad \frac{\partial c_{D,OH^-}}{\partial y_D}=0@\,y_D=0$$

$$c_{D,p}=1@\,t_D=0$$
$$c_{D,H^+}=1@\,t_D=0$$
$$c_{D,OH^-}=1@\,t_D=0$$

1.4.3 Polymer rheology correlation

The polymer gel acts as a non-Newtonian fluid that can be captured by Herschel-Bulkley model. The experimental results verify the credibility of this model to capture the rheological behavior of the microgel. Apparent viscosity of polymer gel can be calculated as

$$\mu_{apparent} = \frac{\sigma_y}{\dot{\gamma}} + K\dot{\gamma}^{n-1} \quad , \tag{25}$$

where yield stress (σ_y), consistency index (K), and power law index (n) are dependent on polymer concentration and pH among other parameters:

$$\sigma_y = f\left(c_p, pH\right)$$
$$n = f\left(c_p, pH\right)$$
$$K = f\left(c_p, pH\right)$$

The rheology parameters (σ_y, K, and n) can be obtained on the basis of the rheology measurements (**Fig. 24**). These measurements are explained in results and discussions section. The following correlations have been developed to capture the polymer gel behavior:

$$\sigma_y = (-3.9617c_p)(pH-2)^2 + (43.579c_p)(pH-2), \tag{26}$$

$$K = (-1.1343c_p)(pH-2)^2 + (12.477c_p)(pH-2) + 0.001, \tag{27}$$

$$n = 0.37, \tag{28}$$

where σ_y (yield stress) is in Pa, K (consistency index) is in Pa.s$^{0.37}$, c_p (polymer concentration) is in wt%. A comparison of the calculated values of these parameters and experimental measurements is shown in **Fig. 24**. The correlations are valid in the pH window of 2-13; the lower extreme corresponds to pH of polymer during injection (pH~2.5) and the higher extreme corresponds to the maximum pH of aqueous solution in contact with cement (pH~13). The values of yield stress, consistency index, and power-law index are 0 Pa, 0.001 Pa.s, and 1, respectively at pH of 2 and lower as wells as at pH of 13 and higher, which means the fluid behaves like water at these extremes. We also ensured that the value of n is equal to (or close to) 1 at low polymer concentrations (less than 0.2 wt%). At these low polymer concentrations fluid behaves like water.

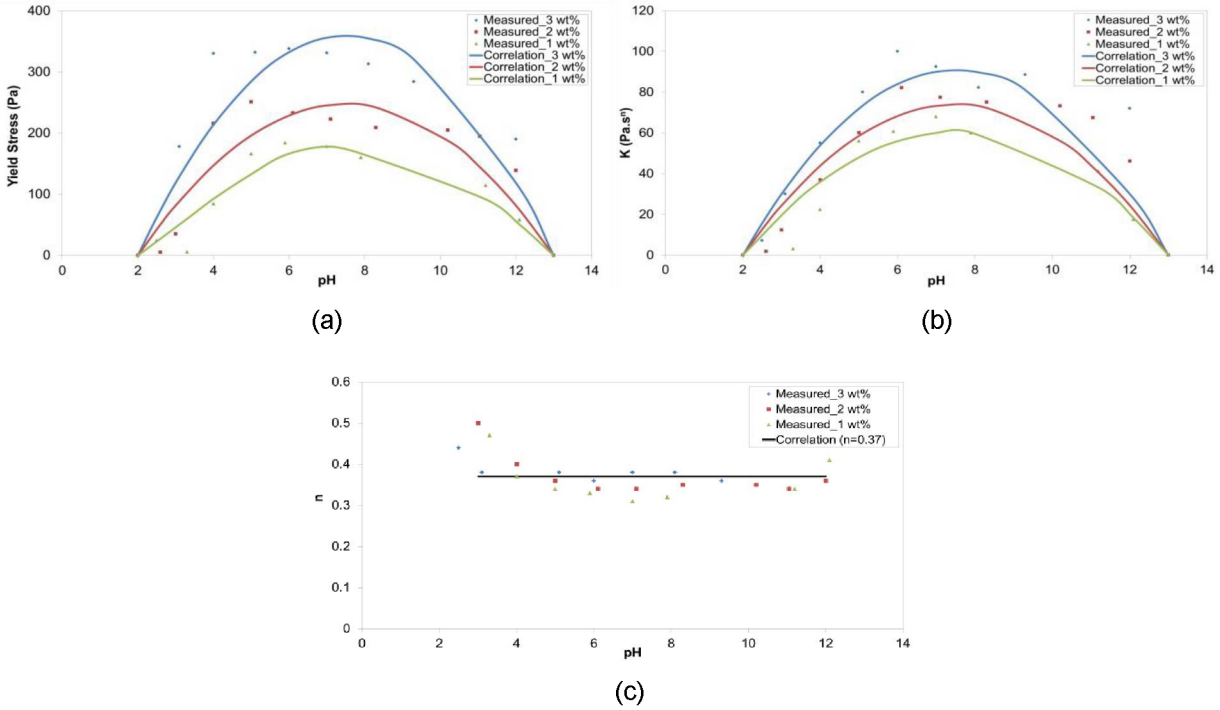

Fig. 24 – Comparison of laboratory measurements and calculations based on correlations (Eq. 13-15) of rheological parameters, (a) yield stress, (b) consistency index, and (c) power-law index, versus pH at different polymer concentrations.

1.4.4 Diffusion coefficients

Hydroxide and proton concentrations are key sources for pH in the reacting polymer solution. The pH can then be used with polymer concentration to predict the Herschel Bulkley parameters (σ_y, K, n) to accurately characterize viscosity of gel. To calculate the concentrations of hydroxide, proton, and polymer in the cement fracture, it is necessary to determine the diffusion coefficient that describes the relative movement and distribution of these molecules.

The Stokes-Einstein equation estimates the diffusion coefficient of a macroscopic particle of radius, r, undergoing a Brownian motion to the viscosity of the fluid in which it is immersed. With the significant difference in the molecular size of hydroxide and swollen gel, one can assume no-slip condition at the interface of both species. The diffusion coefficient of hydroxide ion and swollen gel can be expressed as:

$$D_{OH^-,gel} = \frac{k_B T}{6\pi r}\frac{1}{\mu_{gel}} \quad , \tag{29}$$

$$r = \left(\frac{3MW}{4\pi N \rho}\right)^{1/3} \quad , \tag{30}$$

where $D_{OH-,gel}$ is the diffusion coefficient of OH^- ions in the swollen gel, μ_{gel} is the swollen gel viscosity, r is the hydrodynamic radius of hydroxide ion, k_B is the Boltzmann constant, and T is the temperature of the solution environment. The diffusion coefficient of OH^- is inversely proportional to gel viscosity, which means that as polymer gels up it becomes difficult for more OH^- to diffuse and increase the pH above the optimal pH. In addition, an empirical diffusivity equation was developed and correlated with lab results for Carbopol 940 (A-sasutjarit et al. 2005):

$$D_{ion-gel} = 0.0659 / \mu_{apparent} + 9 \times 10^{-5} \quad , \tag{31}$$

where $D_{ion,gel}$ is the diffusion coefficient between ion and gel. This equation also suggests the inverse relationship between diffusivity and gel viscosity, but shows that diffusivity will asymptote to a constant value at higher viscosities due to the reduction of free volume and the impediment of ion mobility.

For sealing micro-fractures in cement, only a small concentration of polymer is required to achieve significant yield stress. Studies have shown that the diffusivity has an inverse dependence on polymer molecular weight for solutions with low concentration of solid microgel particles (Bird et al. 1987). The diffusion coefficient for polymer solution can be expressed as

$$D_{polymer-solvent} = \frac{1}{MW_{polymer}} \quad , \tag{32}$$

where $D_{polymer\text{-}solution}$ is the diffusion coefficient of polymer microgel dispersion, and $MW_{polymer}$ is the molecular weight of microgel particles.

2 Results and Discussions

In this section, we provide the results of polymer rheology measurements, laboratory experiments, and simulations.

2.1 Polymer Rheology Measurements

As mentioned earlier, polymer dispersion is found to have good fit with the Herschel-Bulkley model, which exhibits both shear-thinning (power law) behavior and a yield stress. Yield stress is measured dynamically in a rheometer by extrapolation to the y-intercept of a stress versus shear rate curve (similar to Figs. 6-7). The apparent viscosity (Eq. 25) is dependent upon those Herschel-Bulkley parameters and the shear rate of the fluid. Since the polymer dispersivity can change due to changes in viscosity as a result of pH variation, these Herschel-Bulkley parameters are in turn a strong function of the solution's pH among other parameters.

2.1.1 Polymer behavior vs. pH

Fig. 25 shows the polymer yield stress significantly increases over pH values from 3 to 5 and remains relatively high at pH value between 5 and 10. **Fig. 26** is the measurement of consistency index (*K*) and power law index (*n*), measurements for various pH. Note that the trend in *K* very much resembles that of in the previous figure and *n* is seen to remain relatively constant over various pH and concentrations.

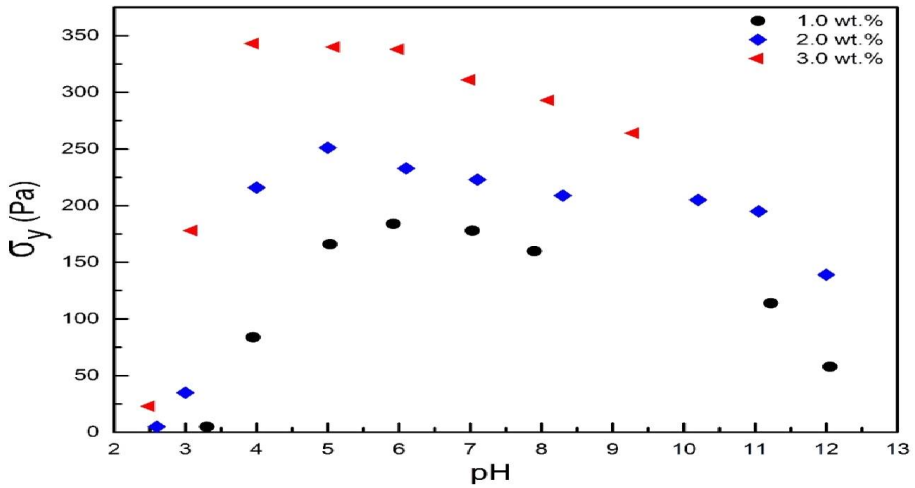

Fig. 25 – Yield stress measurement at various pH for 1-3 wt % Carbopol 934 (Shafiei et al. 2016).

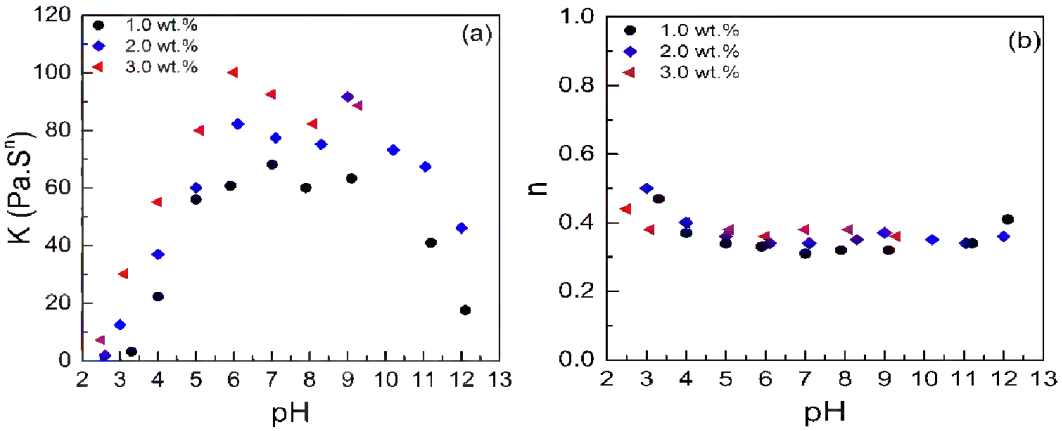

Fig. 26 – Consistency index, *K*, and power law index, *n*, measurements at various pH for 1-3 wt % Carbopol 934 (Shafiei et al. 2016).

2.1.2 Polymer behavior vs. salinity and hardness

Rheology tests (**Fig. 27**) have been done using 3 wt% Carbopol 934 that show yield stress significantly decreases with the increase of calcium content. The presence of divalent calcium cations in cement can destabilize gel structure and greatly compromises the gelant ability to block fluid flow. Therefore, chelating agents as well as a mineral dispersion, were investigated in order to remove or stabilize divalent calcium ions from the cement surface zone. They were either used as additives in polymer solutions or injected alone as pretreatment for the subsequent polymer injection. Furthermore, effects of salinity on polymer rheological parameters of 3 wt% Carbopol 934 were investigated (**Fig. 28**). As can be seen, polymer gel strength reduces at higher salinities.

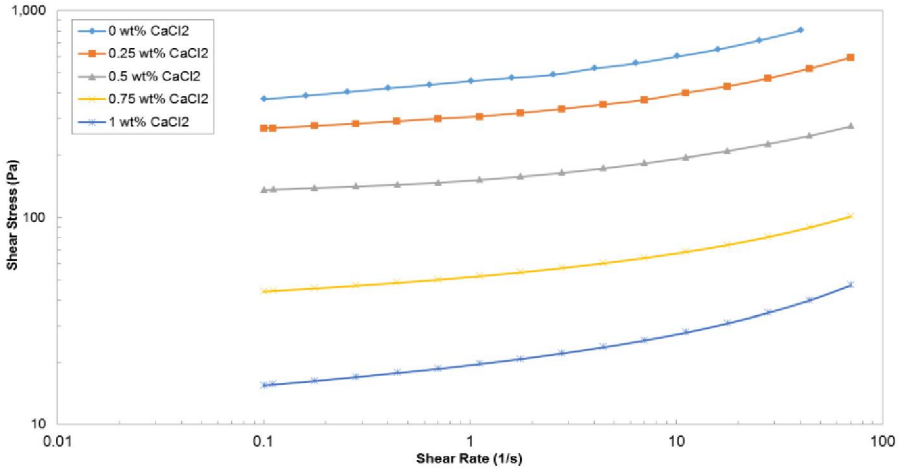

Fig. 27 – Effect of $CaCl_2$ on polymer gel shear stress.

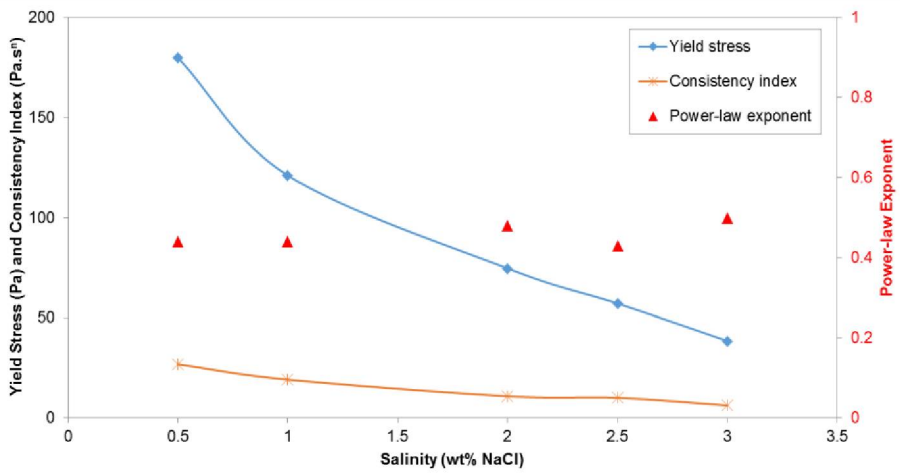

Fig. 28 – Effect of NaCl on rheological parameters of the polymer gel.

2.1.3 Polymer behavior vs. temperature

Polymer rheology was measured at the higher temperature (75 °C) and reported in **Fig. 29**. This figure shows polymer (aqueous solution) maintains its mechanical properties if temperature is high but not close to the water boiling point in which solvent evaporates. To measure the effects of temperature at much higher temperatures close to 100 °C and above, a pressurized sealed system is required to prevent evaporation while measuring the rheological data.

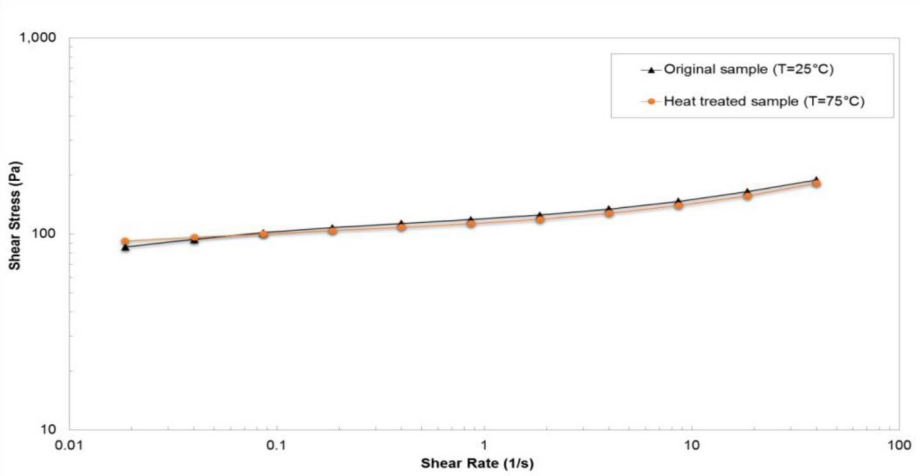

Fig. 29 – Effect of temperature on polymer gel rheology.

2.2 EXPERIMENTAL RESULTS

In this section, we provide the experimental results of the effect of syneresis, chelating agent selection, and coreflood experiments.

2.2.1 Effect of syneresis

As mentioned earlier, Polymer gels undergoing syneresis have difficulty of maintaining gel stability. The presence of divalent cations in cement destabilizes gel structure and greatly compromises the gelant mechanical strength to block fluid flow in the application of sealing cement fractures. This section explains the formation of calcium syneresis and its detrimental effects on the gel used as sealant.

Three types of polymer gel formation were visually distinguished as polymer reacted with the cement fractures. These gel types exhibit different behavior and form in a sequence under the influence of hydroxide and calcium cations. The stages of polymer syneresis can be identified in a static dunk test as described here:

Slightly opaque polymer solution: is the unswollen microgel solid dispersion that is first observed passing through the fracture gap. This acidic dispersion is slightly viscous, nevertheless flows quickly and easily on the cement surface.

Clear solid-like gel: is the swollen microgel deposited on the fracture surface, as the pH of the dispersion is increased, in an immediate reaction with the OH^- leaching out from the cement. This clear microgel deposit is a rather short transition stage but exhibits large yield stress that can greatly reduce flow during injection.

White-syneresed polymer: begins to form after the clear gel formation, due to the subsequent Ca^{2+} leaching out from the cement. Reaction with Ca^{2+} collapses of the structure of the swollen microgel and yields a white-calcium precipitation starting from the cement surface. Continuous supply of calcium ions can happen gradually over time and are seen to cause the remaining clear gel to expel all of its water until separate layers of water and syneresed-polymer is formed.

It is important to distinguish the above three states, as the key to maintaining effective seal depends on maximizing the deposition of clear swollen gel and minimizing the formation of the syneresed Ca-polymer complex.

The gradual syneresis on the surface of the untreated cement can happen over the course of time as the reaction reaches completion. It is an unstable form of polymer gel, and can easily detach on its own or is stripped away by fluid flow in the fracture. This behavior can be explained with the cement-cement fractures, as illustrated in **Fig. 30** (Patterson 2014).

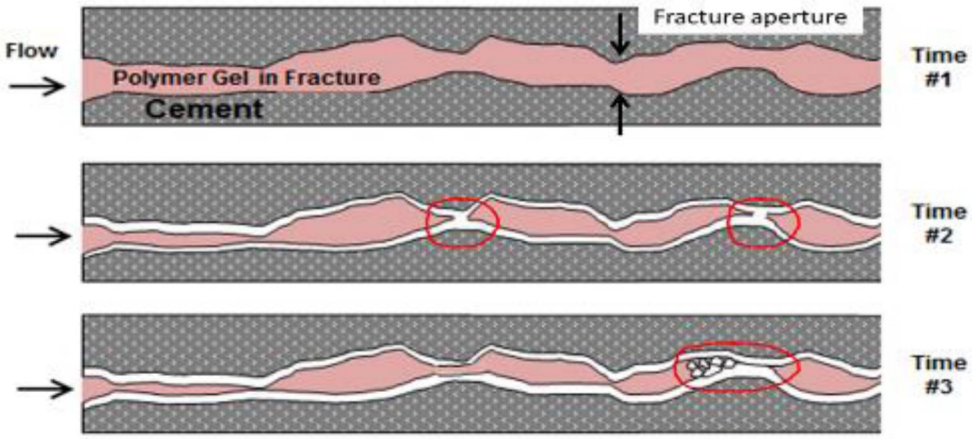

Fig. 30 – An illustration of the polymer syneresis reaction in the cement fracture over time. The syneresed polymer (white precipitation) starts depositing as soon as polymer dispersion (red) is in contact with the untreated cement. Syneresed polymer is an unstable semi-solid that contracts over time, and can easily detach on its own or be stripped away by fluid flow in the fracture. Cyclical blockage and fluid breakthrough were often observed during polymer injections in the untreated cores. Early blockage by syneresed polymer during polymer injection may prevent the polymer from reaching all of the pathways that require proper seal; in addition, the detachment of syneresed polymer from time to time may re-open pathways for fluid flow (Patterson 2014).

Early blockage by syneresed polymer during polymer injection may prevent the polymer from reaching all of the pathways that require the proper seal; in addition, the detachment of the syneresed polymer from time to time may re-open pathways for fluid flow. Due to the irregularity of the flow channels formed in these rough-walled fractures (both in sawed and Brazilian fracture), cyclical blockage and fluid breakthrough occurred during polymer injections. As a result, polymer

injectivity was poor. Furthermore, cores exhibiting the syneresis effect typically were not able to hold back pressurized fluid over long periods of time, which easily broken through at lower pressure gradients.

Table 2 lists the results of several liquid breakthrough tests that were carried out with the polymer placement in untreated cores. Even when successfully placed, the gel was only able to hold back a few psi/ft (F-9, F-12, FP-26 and FP-27) while most cores experienced liquid breakthrough immediately due to the presence of unstable syneresed polymer inside the fracture.

Table 2 – Maximum holdback pressure gradients recorded in liquid breakthrough tests (DI water) for untreated cement cores (F-9, F-12 and F-14) and HCl (pH 2.2) pretreated cement cores (FP-26 and FP-27). These cores had relatively successful polymer placements, despite syneresis observed in all of them, and the fracture remained blocked before performing the breakthrough test. While core F-14 was able to hold back 40 psi/ft due to its higher polymer concentration at 4.5 wt%, most untreated cement cores injected with 3 wt% Carbopol 934 were only able to hold back a few psi/ft. Cores pretreated with HCl had similar holdback pressure gradients as the untreated cores. HCl was unsuccessful in inhibiting syneresis and has shown to increase fracture aperture, also, leaving behind large amounts of oxidized iron precipitation (Patterson 2014).

Core Type	Experiment	Aperture (mm)	Injected Solution		Shut-in Time	Holdback Pressure Gradient (psi/ft)
			Polymer (wt%)	NaCl (wt%)		
Cement-cement	F-9	0.336	3	0.5	4 days	6.5
	F-12	0.271	3	0.5	4 days	7.2
	F-14	0.359	4.5	0.5	4 days	40
Cement-Plastic	FP-26	0.314	3	--	24 hours	2.6
	FP-27	0.229	3	--	24 hours	8

2.2.2 Chelating agent selection

The chemical reactions between syneresis inhibitors and cement, as well as between polymer gel and formation fluids have a significant influence on the design of procedures. This section discusses the application and effectiveness of each syneresis inhibitors, and the effect of acidic formation fluid once the gel is placed, to understand their effect on polymer injection and resulting gel-in-place. In order to prevent syneresis, several chemicals were sought and tested to remove the calcium content from the cement and stabilize gel strength. The following discusses each of their performances:

Laponite as polymer additive. The addition of Laponite into polymer dispersion while adding acid to reduce the final pH exhibited much potential during polymer injection seen in **Fig. 31**. The pH= 2.7 nanocomposite microgel mixture can be seen to be developing some viscosity as it reacts with cement while maintaining only a relatively small pressure drop of a few psi over the course of almost an hour. This indicates that reaction between cement and mixture occurs rather gradually and uniformly because gel slowly deposits causing pressure drop to increase slightly as flow area is reduced. Photos taken during injection show no sign of calcium syneresis and correspond to the start of rapid pressure buildup (at 60 minutes) when polymer dispersion can be seen to have

transformed in to clear gel that occupied the entire fracture. The injection of the mixture ended at 110 minutes showing no sign of syneresis.

After 24 hours of polymer shut-in, white-precipitation can be seen covering the entire cement surface. Upon closer inspection, the precipitation had a grainy texture that was very different from usual rubbery syneresis texture and gradually faded over the course of a week. This indicates that the precipitation may not be calcified gel as syneresis is not reversible. The core was able to hold a static pressure gradient of 2.7 psi/ft over several months without the appearance of syneresis.

The result agrees with another rheology study that showed the strong polymer-clay reaction produced a dense hydrogel network and result in remarkable mechanical performance (Tongwa et al. 2013). This explains why the final product of a clear gel, dense Carbopol 934 and Laponite network, was able to prevent calcium from causing syneresis and maintain seal for a long period of time. Although there are no further tests performed to test the limitations of the Laponite-Carbopol mixture beyond the small static pressure gradient, the addition of the nano-clay is believed to have potential as a stable sealant for blocking buoyant CO_2; and perhaps applications at high temperature conditions (Tongwa et al. 2013).

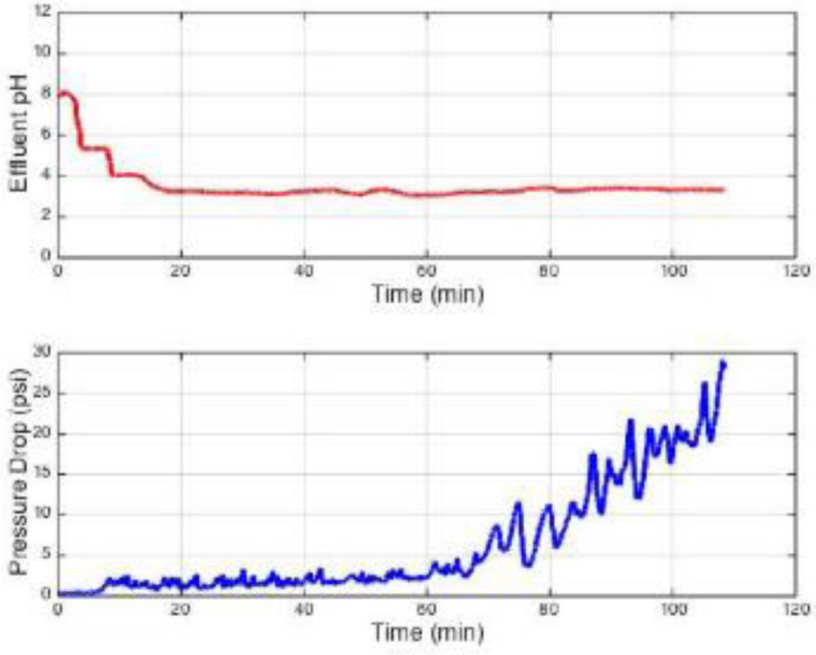

Fig. 31 – Effluent pH and pressure drop recorded during polymer injection in core 6FP-29 (2 wt% Carbopol 934 and 0.2 wt% Laponite).

EDTA as pretreatment. Cement cores treated with EDTA tetrasodium salt showed good result in removal of calcium and prevention of syneresis after polymer placement; however, polymer injection into EDTA treated cores had unstable pressure response due to the fact that EDTA is highly alkaline.

Fig. 32 shows that despite the water preflush before polymer injection, the residual EDTA caused a rapid increase in pressure drop upon contact with polymer. The pressure response remained erratic throughout the polymer injection over the course of 80 minutes, meaning that the reactivity of EDTA is still strong. This may become a problem for sealing leakages in a wellbore since pathways are generally longer than that of in lab scale and injectivity may be compromised before polymer reaches the target zone.

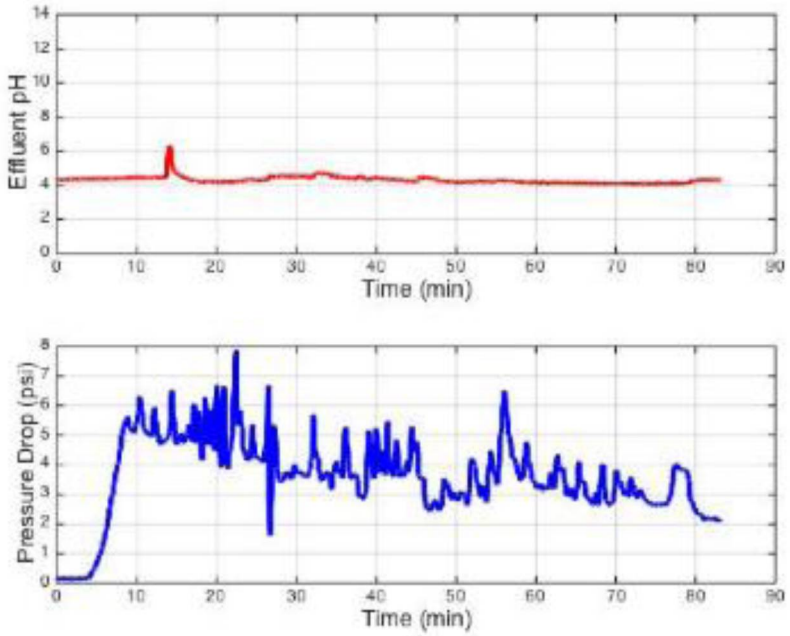

Fig. 32 – The effluent pH and pressure drop recorded during polymer injection of 6FP-31 (3 wt% Carbopol 934 after EDTA pretreatment).

Sodium triphosphate ($Na_5P_3O_{10}$*) pretreatment.* Use of sodium triphosphate ($Na_5P_3O_{10}$) for pretreatment provided effective calcium control and inhibited the formation of syneresed polymer. Cement fractures pretreated with $Na_5P_3O_{10}$ maintained good polymer injectivity and greatly improved the long-term strength and stability of the gel in place. During polymer injection in $Na_5P_3O_{10}$ pretreated cores, the effluent pH steadily decreases. The pressure drop also decreases as shown in **Fig. 33**. This indicates that the decreasing viscosification of the polymer dispersion with time is reducing the pressure drop more than the pressure drop increase by flow channel constriction.

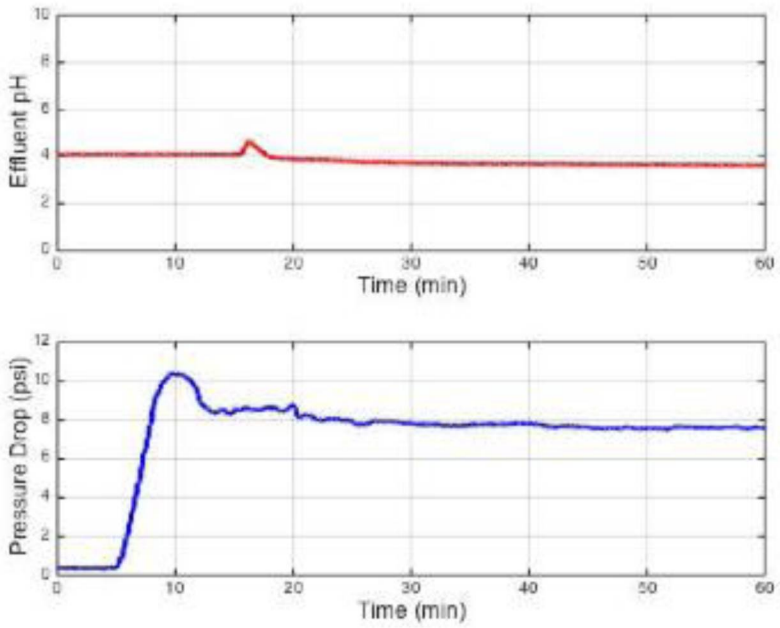

Fig. 33 – The effluent pH and pressure drop recorded during polymer injection of 6FP-34 (3 wt% Carbopol 934 after 24 hr $Na_5P_3O_{10}$ pretreatment).

Hydrochloric acid preflush. Preliminary hydrochloric acid preflush had been tested in an attempt to remove calcium ions from fracture surface (Patterson 2014). In Patterson's work, cores pre-flushed with acid generally resulted in aperture enlargement and the formation of rust-colored iron precipitation. In some cases, the injection of acid can reduce aperture by dissolving calcium content in cement and transporting it further into the fracture to form calcite precipitation. However, his experiments have proven that hydrochloric acid preflush only partially reduced calcium syneresis which has relatively limited improvement in maintaining polymer gel strength and stability (**Fig. 34**).

Fig. 34 – Hydrochloric acid (pH 2.29) preflushed cement core (6FP-27) after 24 hours polymer shut-in. White calcium precipitation with rust-colored precipitate (Patterson 2014).

Among the several syneresis inhibitors tested, it was determined that sodium triphosphate ($Na_5P_3O_{10}$) had the best performance when used as a pretreatment for cement cores. Cement cores pretreated with $Na_5P_3O_{10}$ not only inhibited polymer syneresis but also showed good injectivity and promising gel strength. The resulting holdback pressure gradients for pretreated cores were orders of magnitude higher than the few psi/ft measured for untreated cores and yielded better safety margin for the sealant design based on the 0.2-0.4 psi/ft holdback pressure requirement for a rising CO_2 leakage. In addition, multiple experiments showed that the calcium removal reaction of $Na_5P_3O_{10}$ and cement surface is very quick. This allowed pretreatment procedures to shortened from 24 hours to as brief as 10 minutes while maintaining desirable gel strengths; hence, use of $Na_5P_3O_{10}$ can greatly improve operational efficiency and results in less rig time. Therefore, the rest of experiments were performed using $Na_5P_3O_{10}$ as the chelating agent for pretreatment.

2.2.3 Coreflood experiments

Coreflood experiments are comprised of three stages: (1) pretreatment and soaking, (2) polymer flood and shut in, and (3) flow initiation test. The following subsections explain the experimental results obtained during each stage.

2.2.3.1 Pretreatment

Cores pretreated with sodium triphosphate ($Na_5P_3O_{10}$) have proven to be effective at inhibiting syneresis and improving gel strength by both visual observation and gel strength tests compared to untreated cores. It was originally thought that the cement cores pretreated for longer durations would result in higher gel strength. Some of the earlier cores were all subjected to a standard 24-hour pretreatment.

In order to improve the procedure efficiency, the optimal pretreatment time was sought. Later experiments were designed to pretreat cement cores for 12 hours, 6 hours and 10 minutes. Several subsequent gel strength tests were not affected by the longer treatment time, in fact, some results show that pretreating cores as less as 10 minutes were sufficient to inhibit syneresis. **Fig. 35** presents the results from gel strength tests were subjected to the same polymer shut-in times showed that there is perhaps no correlation between pretreatment time and gel strength. This suggests that $Na_5P_3O_{10}$ pretreatment reacts fast with the calcium ions close to the cement surface. Quick procedures using shorter $Na_5P_3O_{10}$ pretreatment time is ideal and allows for faster leak repairs and better cost efficiency.

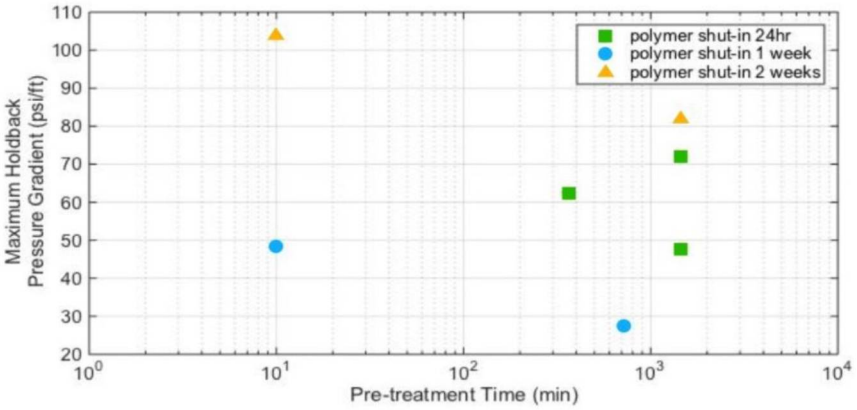

Fig. 35 – Sodium triphosphate ($Na_5P_3O_{10}$) pretreatment time shows no correlation in the improvement of the resulting maximum holdback pressure for subsequent 24-hour, 1-week, and 2-week polymer shut in.

2.2.3.2 Polymer flood

Polymer was injected into cores pretreated with $Na_5P_3O_{10}$ and soaked for enough time (about 24 hrs). Then, we shut-in the core to let the polymer gel up and form a uniform gel through the fracture. The dehydration of gel deposit was observed in many cores that had polymer shut-in time over a course of weeks. Subsequent gel strength test revealed that dehydrated gel poses no harm to gel strength and long-term stability. Most tests have shown that the gel-in-place can develop a much stronger seal as the gel matures. Two sets of experiments under 10-minute and 24-hour pretreatment time are compared in **Fig. 36**. Both sets of data showed an increase in the maximum holdback pressure as polymer shut-in time is increased. This result is very suitable and desirable for sealing purposes since the ultimate goal is for the gel in cement fractures to remain stable and strong long after the injection procedure.

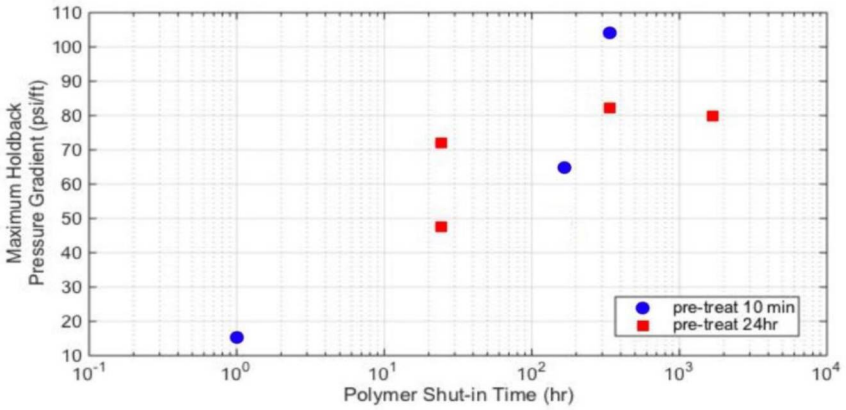

Fig. 36 – Maximum holdback pressure increases as a function of polymer shut-in time for cores pretreated with STP for 10 minutes (6CF-39, 10FP-40, 10FP-41, 10FP-42) and cores pretreated with STP for 24 hours (6FP-34, 6CF-36, 10FP-36).

2.2.3.3 Flow initiation test

We presented the experimental procedure and setup for flow initiation tests using DI water/acidic brine and (low/high pressure) CO_2 injection. This section provides the results of 18 cement corefloods and 2 cement annulus bench tests. Labeling of each coreflood is based on the cement length, core construction and the order the experiment was performed. The label starts by using numbers to specify the length (in inches) of the core (e.g., 6FP-34 is 6" and 10FP-36 is 10"); then followed by letters to indicate the type of core construction (e.g., 6CF-36 is a cement-cement fracture core, 10FP-36 is a cement-plastic plate core, and 6CHass-1 is a cement coreflood performed in the Hassler coreholder). Lastly, the number following the dash indicates the sequence in which the coreflood was performed. We monitored the pressure data, effluent pH, and visual observations from all the corefloods and cement annulus tests. The experimental results were further used to understand the sealing mechanisms and the parameters that control the sealing behavior.

Table 3 is a detailed summary of the experiments using $Na_5P_3O_{10}$ under various pretreatment times, polymer shut-in time, and the holdback fluid employed. The gel strength tests after 24 hours of shut-in for the $Na_5P_3O_{10}$ pretreated cement cores held back an average of 60 psi/ft of water under standard conditions and held back 150-3000 psi/ft under supercritical conditions. This is compared to the cores without pretreatment (6FP-35 and cores in Table) held back an average of 14.2 psi/ft. Cores pretreated with $Na_5P_3O_{10}$ showed no signs of polymer syneresis later in long periods of shut in.

Table 3 – A summary of sodium triphosphate ($Na_5P_3O_{10}$) pretreatment and gel strength testing results. Cement cores in this table were pretreated with 14.5 g/100 mL $Na_5P_3O_{10}$ from 10 minutes up to 24 hours, then injected with 3 wt% Carbopol 934 polymer dispersion and allowed polymer shut-in from 1 hour up to 10 weeks. Various holdback fluids were used in the liquid holdback test to obtain the maximum holdback pressure gradient (psi/ft); the acidic brine was made by adding HCl acid into 2 wt% NaCl until the solution reached pH=4 measured by the pH meter. For 6Hass-1, CO_2 gas was injected at room temperature and held above 60 psi/ft constant pressure for 8 weeks and was followed by a gel strength test using acidic brine. Individual core lengths are marked in the number at the beginning of the test number.

Core Type	Test	Fracture Aperture (mm)	Pretreatment Time	Shut-in Time	Max Holdback Pressure Gradient (psi/ft)	Holdback Fluid
Cement-cement	6CF-36	0.436	24 hours	2 weeks	82.3	pH 4 brine
	6CF-39	0.463	10 minutes	2 weeks	104.1	pH 4 brine
Cement-Plastic	6FP-33	0.138	As an additive	24 hours	56	DI water
	6FP-34	0.159	24 hours	24 hours	72	DI water
				10 weeks	80	DI water
	10FP-35	0.218	--	1 week	21	DI water
	10FP-37	0.209	12 hours	1 week	27.6	DI water
	10FP-36	0.255	24 hours	24 hours	65	DI water
	10FP-38	0.228	6 hours	24 hours	62.4	DI water
				5 weeks	39.6	DI water
	10FP-39	0.277	6 hours	5 weeks	50.4	DI water
	10FP-40	0.547	10 minutes	1 week	48.4	pH 4 brine
	10FP-41	0.530	10 minutes	1 hour	15	DI water
	10FP-42	0.525	10 minutes	1 hour	15.4	pH 4 brine
Hassler coreholder	6Hass-1	0.423	10 minutes	24 hours	> 60	CO_2 gas
			10 minutes	8 weeks	160	pH 4 brine
	6Hass-2	0.213	10 minutes	24 hours	150	Supercritical CO_2
	6Hass-3	0.181	10 minutes	24 hours	3000	Supercritical CO_2

2.2.4 Cement annulus bench tests

The cement annulus bench test injection of polymer in cement pathway is a practical approach in demonstrating the application of pH-triggered polymer sealant in the cement annulus (**Fig. 37**). Experiment PVC-1 (coat hanger channel, 1.167 ft in length) was able to hold back constant pressure gradient of 15 psi/ft for one week without any breakthrough. Then the breakthrough test was done on PVC-1 by slowly increasing the inlet pressure of the compressed air until the bench test was broken through at 62 psi, which corresponds to pressure gradient of around 63 psi/ft. This holdback pressure gradient of the bench test PVC-1 is in the expected range of gel's sealing performance at shallow reservoir depths. Previous corefloods, that had polymer shut-in time longer than one week under standard condition, have shown to have an average holdback pressure gradient very close to PVC-1.

Experiment TYG-1 (fractured cement in Tygon tubing, 1.25 ft in length) was also able to hold back constant pressure gradient of 15 psi/ft for one week without any breakthrough. The same breakthrough test was done on TYG-1 and it held a pressure gradient of 25.6 psi/ft before compressed air broke through. This pressure gradient is sufficient for the requirement of holding back a few psi/ft corresponding to rising buoyant CO_2; however, the lower holdback pressure may be the result of the tubing material's expansion response to the pressure increase, which can create gaps between tube wall and cement for the compressed air to breakthrough.

Fig. 37 - Experiment PVC-1 (left) and TYG-1 (right) successfully held 15 psi/ft constant pressure for one week. During pressure breakthrough test, PVC-1 had the maximum breakthrough at 63 psi/ft and TYG-1 (right) had the maximum breakthrough at 25.6 psi/ft.

The flow of the microgel in the fracture can be captured by a slit-flow model. **Fig. 38** illustrates a simplified version of this model for the half of the slit below the centerline. The polymer at a low pH is injected at the inlet. The microgel apparent viscosity increases as soon as it contacts the cement surface as a result of an increase in the pH. The polymer has shown non-Newtonian behavior based on our rheology experiments. Hence, polymer rheology should be captured on the basis of the non-Newtonian behavior observed in the experiments along with transport properties of proton (H^+) or hydroxide (OH^-) and polymer solutes. Diffusive properties of these species are required to model the transport along the fracture and from the wall towards the centerline (perpendicular).

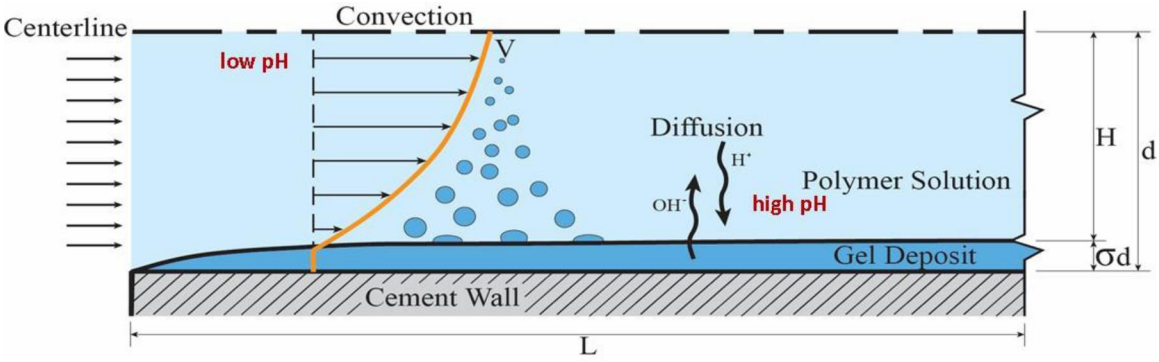

Fig. 38 – Illustration of the flow and boundary geometry.

2.3.1 Comparison with experimental results

We compared our simulation model against coreflood experimental results. The properties of experiment FP-42 are summarized in **Table 4**. **Fig. 23** shows the flow chart for the modeling of the process. The simulation model was validated against recorded pressure gradient in the experiment as well as steady-state flow rate and the time when flow reached to steady state for both polymer injection and water breakthrough tests.

Table 4 – Summary of Experiment Properties.

Experiment ID	FP-42
Description	Cement-Plastic
Length	10 in. (=0.254 m)
Width	1 in. (=0.0254 m)
Aperture	0.525 mm (=0.000525 m)
Polymer concentration	3 wt%
pH at cement surface	12-13
Polymer Injection Test	
Injection rate	3.5 ml/min
pH initial	7
pH inlet	2.5
pH outlet	5
Elapsed time	80 min
Shut-in time	60 min
Steady-state pressure gradient	16 psi/ft
Water Breakthrough Test	
Injection rate	0.5 ml/min
pH initial	5
pH inlet	4
Elapsed time	25 min
Holdback pressure	15.4 psi/ft

2.3.1.1 Polymer flood

The pressure gradient and the effluent pH were recorded during the polymer injection test and plotted in **Fig. 39**. This figure shows the steady-state pressure gradient of about 16 psi/ft with constant injection rate of 3.5 ml/min after almost 50 min.

Fig. 40 shows the simulation results of polymer injection test at the specific applied pressure gradient. **Fig. 41** conveys the same information but with the focus on the region with flow rates below 20 ml/min. Although the experiment was done at constant flow rate, but the simulation was performed at constant pressure gradient because the polymer gel showed compressible behavior during the polymer injection and before it broke through. As seen in **Fig. 40**, with 12 psi/ft pressure gradient, the flow reached to steady state after 50 min. The flow almost ceases to flow with the final flow rate of less than 0.3 ml/min. **Fig. 40** shows that the flow reached to steady state after 50 min with the flow rate of 3 ml/min for the case of 17 psi/ft. This case is comparable with the experiment (Fig. 39) where the flow reached to steady state after almost 50 min with the flow rate of 3.5 ml/min. The pressure gradient recorded in the experiment was inconstant with higher values than 17 psi/ft which might be responsible for the slightly higher flow rate observed in the experiment. This figure also shows the plots for cases with smaller pressure gradients and for the case with ten times larger polymer diffusivity. As seen, lower pressure gradients are not capable to push the polymer into the fracture as soon as it gels up. The case with larger polymer diffusivity shows that higher values of polymer diffusivity results in faster gelation with the same applied pressure gradient.

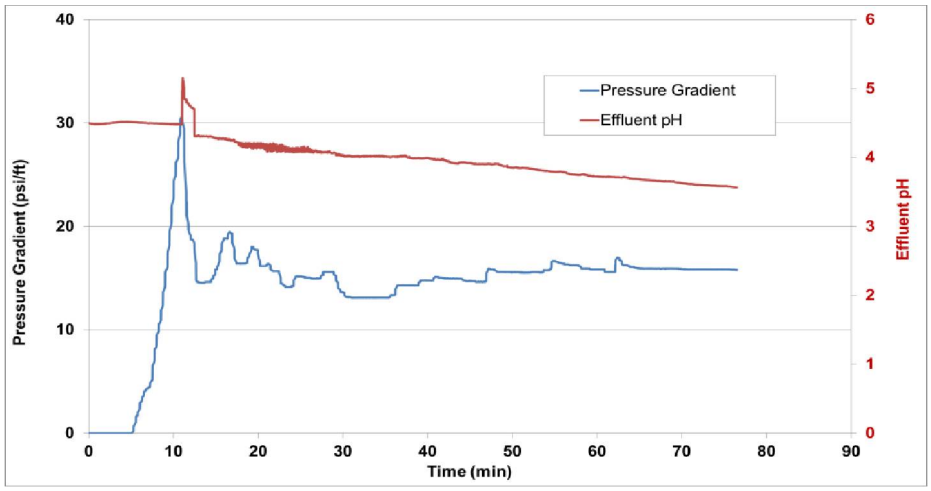

Fig. 39 – Pressure gradient and effluent pH corresponding to the polymer injection test.

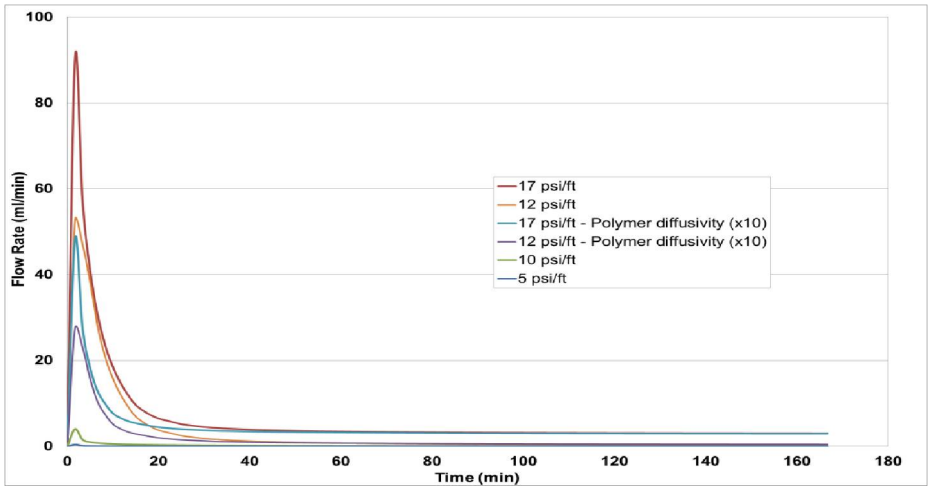

Fig. 40 – Flow rate vs. time for different applied pressure gradients – polymer injection test.

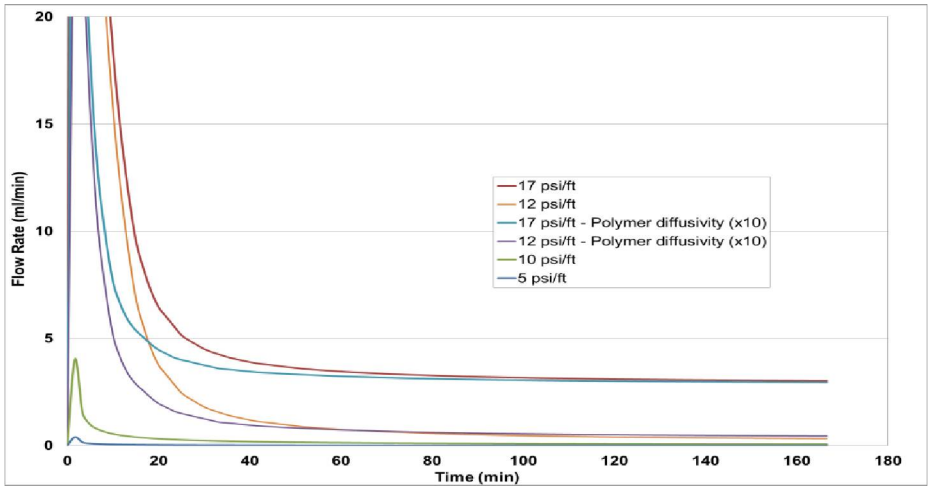

Fig. 41 – Flow rate vs. time for different applied pressure gradients – polymer injection test, region: 0-20 ml/min.

2.3.1.2 Flow initiation test

Fig. 42 shows the pressure gradient versus injection time for the water breakthrough test. The maximum pressure gradient before the polymer gel starts to flow was recorded to be 15.4 psi/ft corresponding to the peak of the plot. Please note that no flow was observed during the first region of the curve (time 3-20 min) before the peak. Although the test was done at constant rate, but the polymer gel was compressed up to 15.4 psi/ft and then broke through. The decline in pressure gradient after the peak confirms the water breakthrough.

Fig. 43 shows the pressure gradient for the simulation with the water injection rate of 0.5 ml/min, similar to the experiment (Table 4). The maximum holdback pressure is 11.2 psi/ft based on the results of this case. This value is pretty close to the holdback pressure observed in the experiment (15.4 psi/ft). The holdback pressure is inversely proportional to the fracture aperture. It is very difficult to maintain a specific aperture in the experiment considering the confining pressure and the geometry of the core. Hence, the aperture reported in the experiment is definitely an average value and its value might not be as accurate. As a result, the uncertainty in the fracture aperture might be the cause of the difference between experimental and simulation results.

Fig. 44 shows the flow rate for the water breakthrough test for different applied pressure gradients. As seen in this figure, the flow is very small below the holdback pressure of 11.2 psi/ft and the flow is much higher for the pressure gradients above this value. Therefore, this observation verifies that the value of 11.2 psi/ft accounts for the holdback pressure and can be compared to the value observed in the experiment.

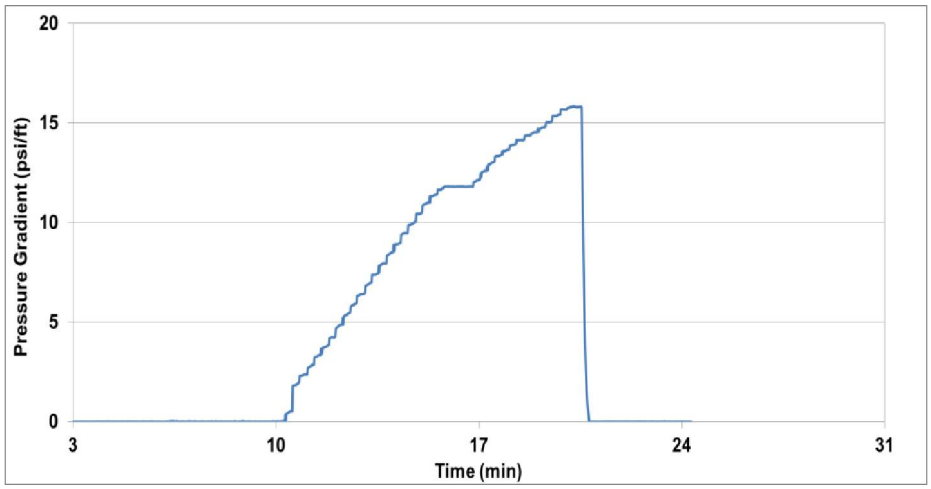

Fig. 42 – Pressure gradient corresponding to the water breakthrough test.

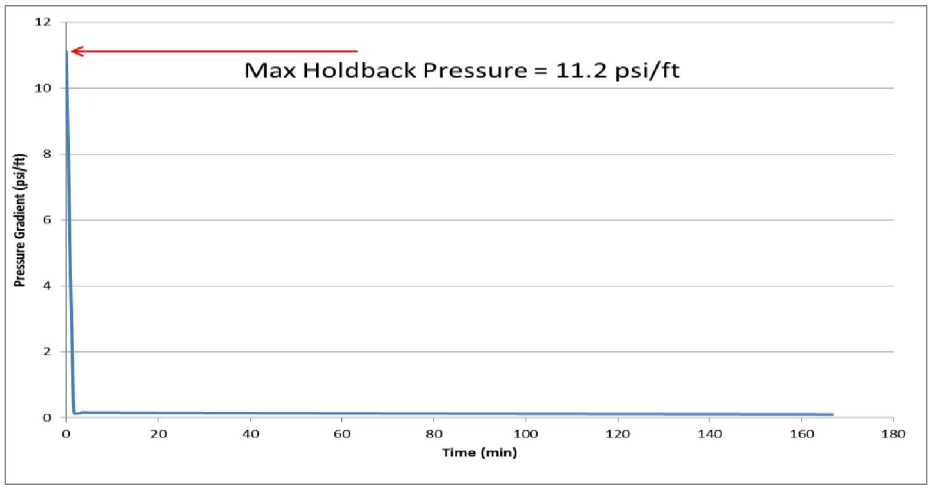

Fig. 43 – Pressure gradient vs. time, the holdback pressure is 11.2 psi/ft – water breakthrough test.

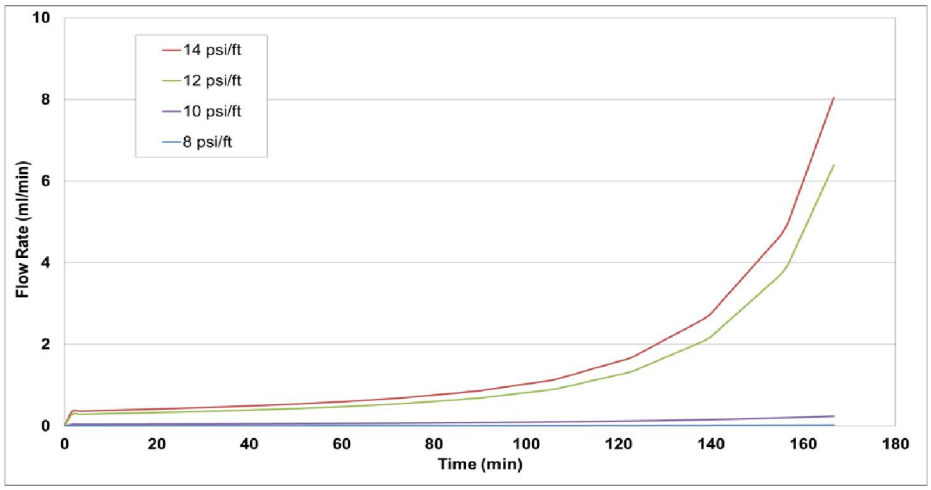

Fig. 44 – Flow rate vs. time at different applied pressure gradients – water breakthrough test.

2.3.2 Sensitivity studies

In this section, we provide the results of the sensitivity analysis of the effects of fracture aperture, formation of the gel deposit layer, polymer concentration, and pretreatment on the performance of the polymer gel to block leakage pathways (Tavassoli et al. 2016).

2.3.2.1 Effect of fracture aperture

The pressure gradient is dependent on the fracture aperture. We are interested to understand how the pressure gradient changes versus the fracture aperture. **Fig. 45** shows the simulation results of the pressure gradient for water breakthrough test at different fracture apertures. The experimental results of the pressure gradient at different fracture apertures are also provided in **Fig. 45**. The simulation and experimental results are in pretty good agreement.

We already know that the pressure gradient increases as the fracture aperture decreases. The plot of the pressure gradient in **Fig. 45** shows the same trend; however, there are two regions where the pressure gradient does not increase as much. The reason for this observation might be the increase in hydroxide diffusion as the fracture aperture decreases, in which hydroxide reaches to the fracture centerline faster. In other words, by reducing the fracture aperture there would be a competition between the increase of pressure gradient due to the decrease in fracture aperture and the decrease of pressure gradient due to the increase of pH beyond 7. The rheological behavior of the polymer gel shows that the yield stress increases up to pH=7 and decreases beyond this point. More insight can be gained by monitoring the pH for these cases.

Fig. 46 shows the hydroxide concentration and dynamic viscosity profile after 170 min for two aperture sizes of 5 and 200 microns. The numerical disturbance can be seen for the aperture size of 5 microns which shows the challenge to model the case at such small fracture sizes. As seen in this figure, hydroxide fills up the fracture much faster in 5 microns fracture than 200 microns one. As a result, pH moves to values above 7 much faster in the smaller fracture and viscosity reduces faster. **Fig. 47** shows pH profiles for four different fracture apertures of 400, 300, 200, and 150 microns after 170 min.

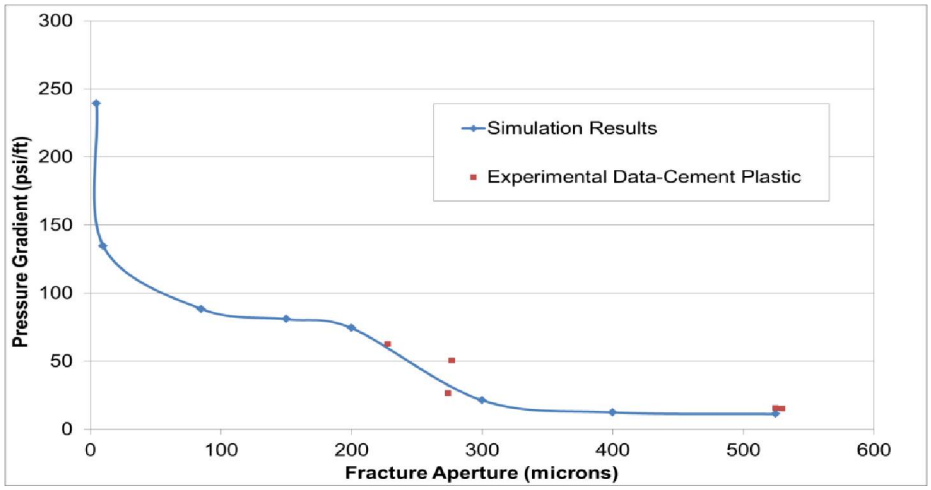

Fig. 45 – Effect of fracture aperture on the pressure gradient – water breakthrough test.

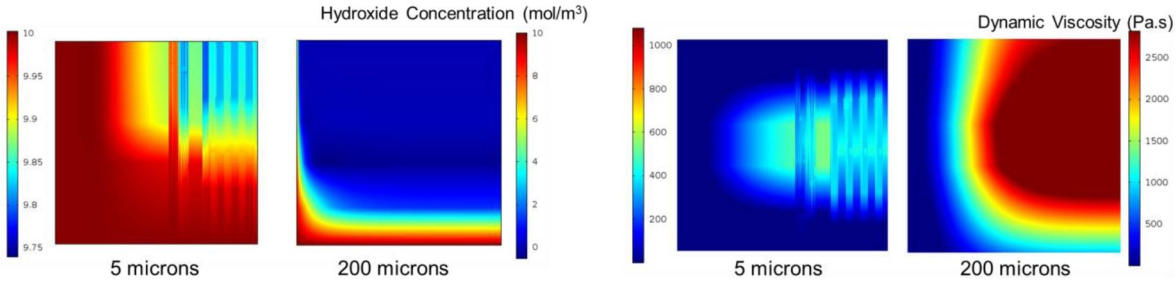

(a) (b)

Fig. 46 – Hydroxide concentration (a) and dynamic viscosity (b) profiles for fracture apertures of 5 and 200 microns at time=170 min - water breakthrough test.

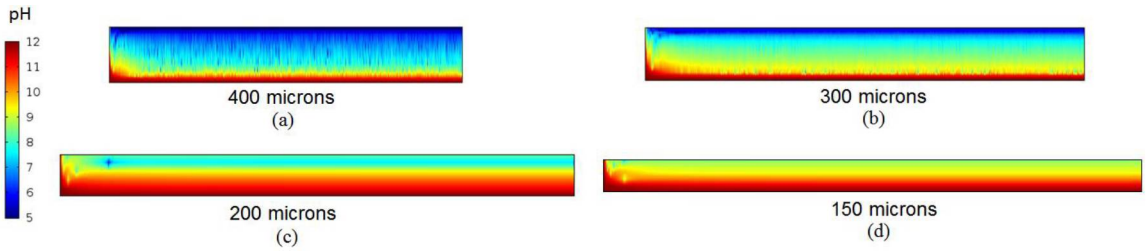

Fig. 47 – pH profiles for fracture apertures of (a) 400, (b) 300, (c) 200, and (d) 150 microns at time=170 min - water breakthrough test; the visualization aspect ratio (aperture:length) = 100:1.

2.3.2.2 Effect of gel deposit layer

The observed trend in Fig. 45 is due to the continuous diffusion of hydroxide ions from the cement wall to the fracture during the polymer injection and shut-in stages. Hydroxide diffusivity might not remain the same through the course of the experiment because of the deposition of gel layer on cement surface.

During the experiment when the microgel dispersion in acidic condition enters into the fracture, the acidic fluid will quickly flush the resident alkaline fluid initially available in the cement fracture. Hydroxide ions in the cement will ooze out and diffuse through the flowing, acidic fluid. As the fluid pH increases above the critical pH, the solid microgel particles will swell. Some of these swollen microgel particles will deposit on cement surface; some others will flow along the fracture; and some others will diffuse into the central acidic zone and shrink back. The deposited swollen microgels will form a gel layer. Hydroxide ions will still diffuse through the gel layer, but at a rate much slower than that through the flowing fluid.

We simulated this case in which a microgel layer deposits on the cement surface. In this simulation case it was assumed that the layer thickness is negligible compared to the fracture and final pH value is equal to pH value measured in the experiment for the polymer effluent. **Fig. 48** shows that polymer enters the fracture and fills up the gap immediately as the size of fracture is extremely small. t_p is polymer breakthrough time, which is about 100 s. **Fig. 49** shows the change of pH for this case. As seen in this figure, polymer solution quickly flushes the initial alkaline fluid and the final solution is acidic with pH of about 2.5. **Fig. 50** shows the dynamic viscosity increases from initially water-like fluid to the viscous polymer gel.

Over the course of time, pH increases due to hydroxide diffusion from the cement surface. **Fig. 51** shows pH profile at later times until the end of polymer flood (t_f=170 min). The final time corresponds to the simulation time in Figs 40 and 41. As we mentioned earlier, in this simulation case we considered formation of a gel layer on cement surface which limits further increase in bulk pH. If we shut in polymer for sufficient time, pH sets to a constant value through the fracture (**Fig. 52**). The shut-in time (t_s) is 24 hours similar to the experimental procedure. The longer shut-in time was selected to make sure that the polymer is completely gelled inside the fracture. Simulation results show that pH reached to a constant value after about 11 hours which is less than half of the shut-in time. This time definitely depends on the diffusion coefficient and size of the fracture. As we previously reported, experimental results with shorter shut-in times have also shown satisfactory results in blocking the fracture.

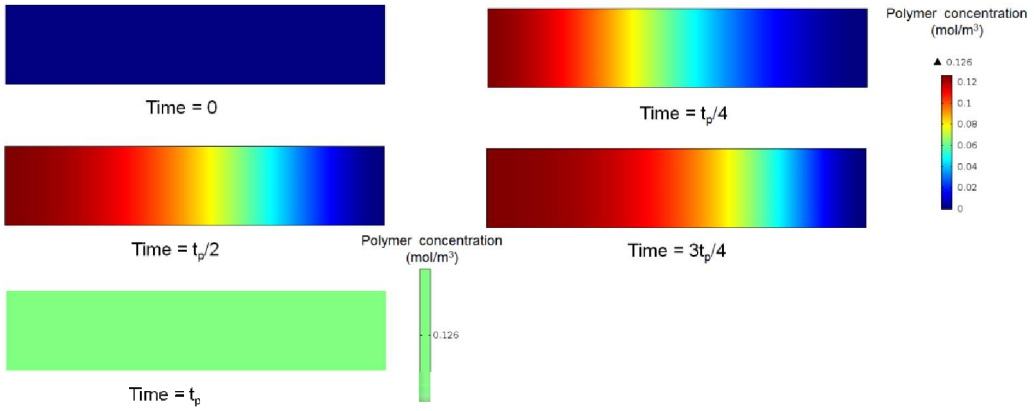

Fig. 48 – Polymer concentration profile – polymer injection test; t_p = 100 s.

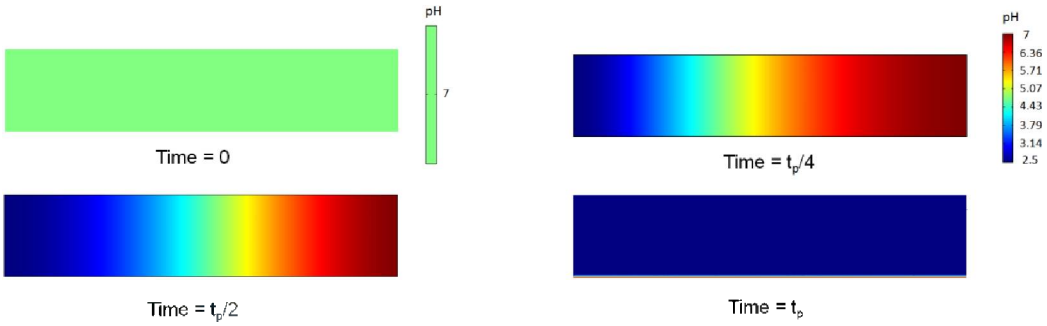

Fig. 49 – pH profile – polymer injection test; t_p = 100 s.

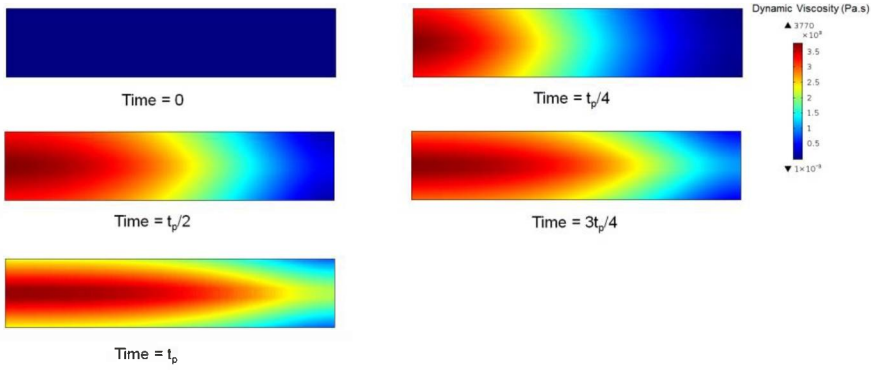

Fig. 50 – Dynamic viscosity profile – polymer injection test; t_p = 100 s.

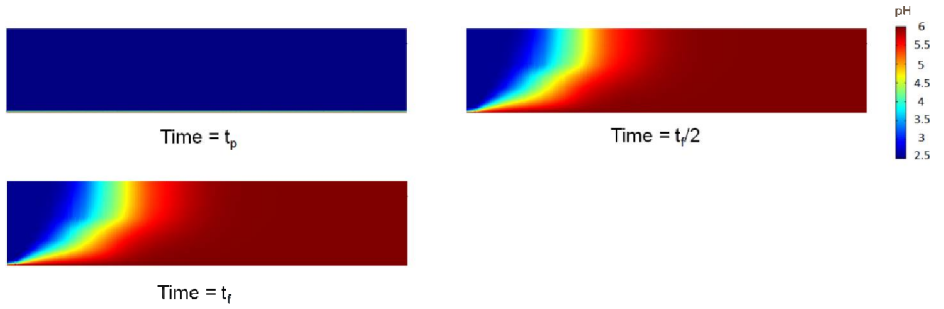

Fig. 51 – pH profile – polymer injection test; t_p = 100 s and t_f = 170 min.

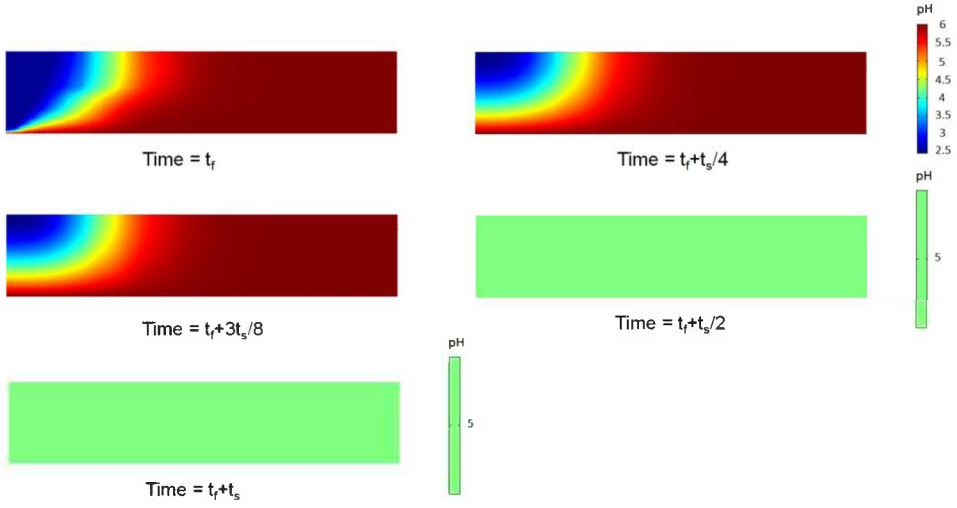

Fig. 52 – pH profile – polymer shut in; t_f = 170 min and t_s=24 hr.

The holdback pressure would be also different in the case of formation of a deposit layer on the cement surface. **Fig. 53** shows the simulated pressure gradient corresponding to the experiment. The maximum holdback pressure was recorded to be 15.4 psi/ft in the experiment (Table 4). **Fig. 53** reports the simulated values of 11.4 and 40 psi/ft for the model without and with the deposit layer, respectively. This result verifies that the deposit layer prevents the continuous increase of pH.

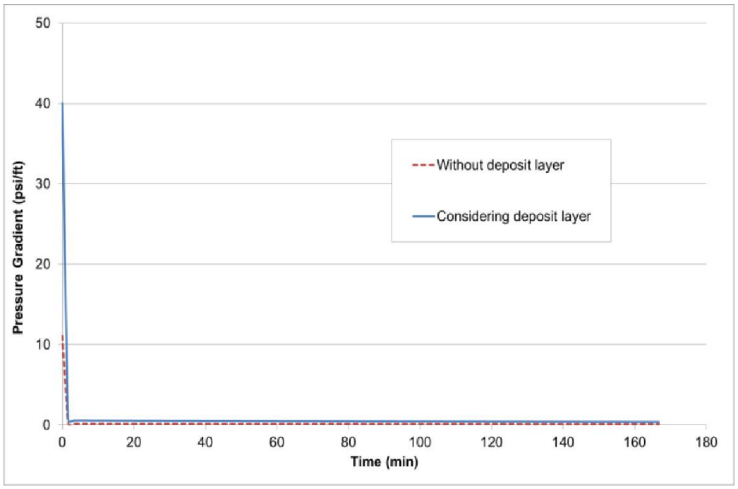

Fig. 53 – Pressure gradient vs. time for the simulation case without a polymer-gel deposit layer on cement surface and for the simulation case considering the deposit layer – water breakthrough test.

The simulated value of 40 psi/ft considering the effect of deposit layer is much larger than the value observed in the experiment; however, larger pressure gradients were observed in other experiments with similar fracture sizes. As it was mentioned earlier there is a strong uncertainty to set the fracture size during experiments. The simulated holdback pressure is in line with the calculated theoretical holdback pressure and polymer rheology (Fig. 24) as discussed below.

The holdback pressure gradients of the gel can be compared with the theoretical pressure gradients calculated from the gel yield stresses measured in polymer rheology experiments. Theoretical pressure gradients can be calculated by

$$\left(\frac{\Delta P}{\Delta L}\right)_{theoretical} = \frac{\sigma_y}{r_H} \quad , \tag{33}$$

where σ_y is the polymer-gel yield stress (psi) and r_H is the hydraulic radius of the aperture calculated by

$$r_H = \frac{WB}{2(W+B)} \quad , \tag{34}$$

where W is the core width and B is the fracture aperture. Eq. 34 can be approximated as in Eq. 35, since $W>>B$:

$$\left(\frac{\Delta P}{\Delta L}\right)_{theoretical} = \frac{2\sigma_y}{B} \quad , \tag{35}$$

Polymer pH is equal to 5 at the end of shut-in stage (Fig. 52). The corresponding yield stress value measured in lab for 3 wt% polymer solution is equal to 340 Pa at pH=5 (Fig. 24). The fracture aperture size in the experiment is 0.525 mm (Table 4). Therefore, the theoretical pressure gradient is calculated using Eq. 35 to be equal to 57.26 psi/ft. This value is comparable to 40 psi/ft. As seen in Fig. 24, a fitting curve was used in the simulation which gives a yield stress of 281 Pa for the

same pH. Using this value the theoretical pressure gradient is 47.3 psi/ft, which is much closer to the simulated value of 40 psi/ft.

We further repeated our simulations to study the effect of aperture size on pressure gradient with consideration of formation of deposit layer. **Fig. 54** shows the comparison of the simulated pressure gradient and experimental values. Recent experiments were performed at low fracture sizes. We also calculated the theoretical pressure gradient similar to the aforementioned calculation. **Fig. 54** compares the simulated, experimental, and theoretical values of pressure gradient versus fracture aperture size. The comparison shows satisfactory results obtained using the simulation model.

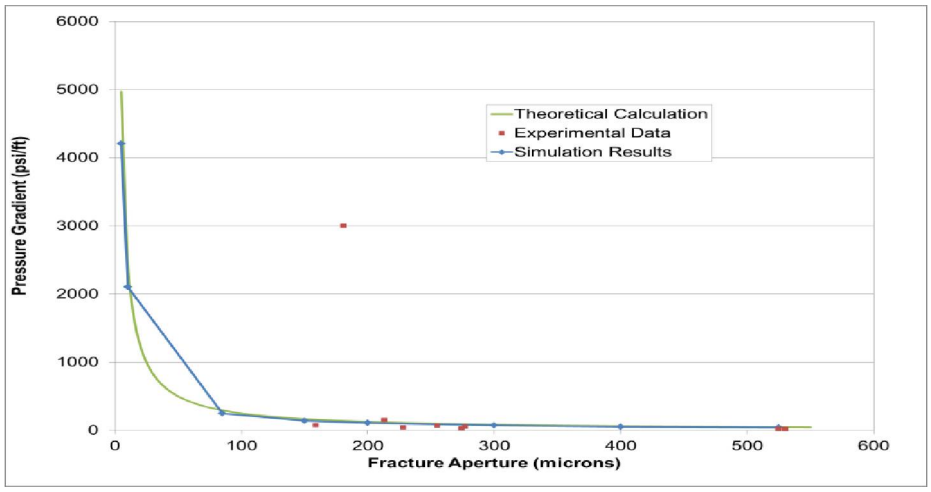

Fig. 54 – Effect of fracture aperture on the pressure gradient; comparison of theoretical, experimental, and simulated values of pressure gradient – water breakthrough test using simulation model considering the formation of gel deposit layer on cement surface.

2.3.2.3 Effect of polymer concentration

We also investigated the effect of fracture aperture size on pressure gradient at different polymer concentrations. **Fig. 55** shows the pressure gradient for four different polymer concentration of 1, 2, 3, and 5 wt%. As seen in this figure, the holdback pressure gradient increases as polymer concentration increases. **Fig. 56** conveys the same information for fracture aperture size larger than 85 microns to better visualize the trend.

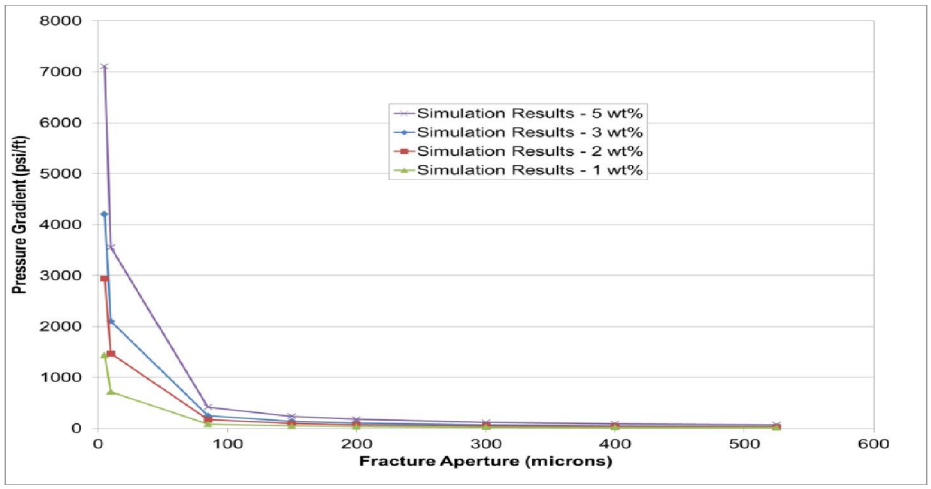

Fig. 55 – Effect of fracture aperture on the pressure gradient at different polymer concentrations – water breakthrough test using simulation model considering the formation of gel deposit layer on cement surface.

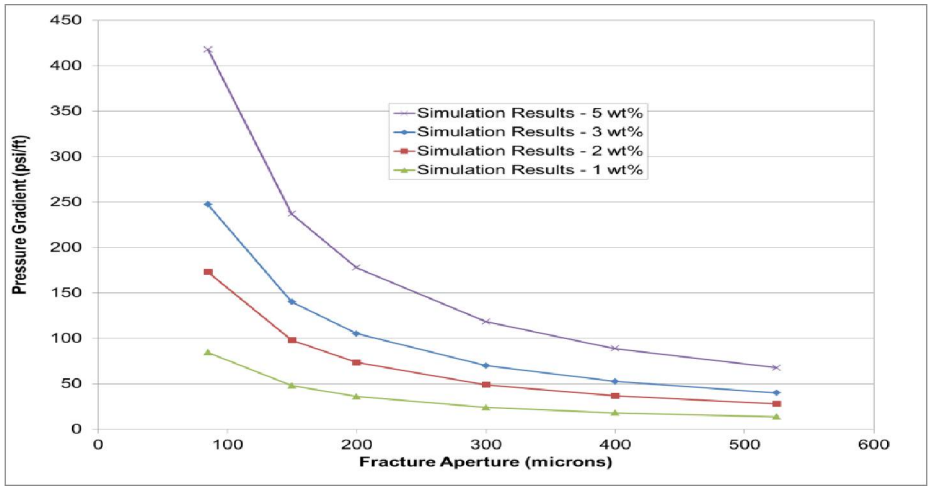

Fig. 56 – Effect of fracture aperture on the pressure gradient at different polymer concentrations – water breakthrough test using simulation model considering the formation of gel deposit layer on cement surface; region above 85 microns.

2.3.2.4 Effect of pretreatment

As mentioned earlier, presence of $CaCl_2$ can be detrimental to gel integrity and its strength to block penetrating-fluid flow. We simulated the case in which $CaCl_2$ are present in the cement fracture before polymer flood, representing the scenario in which cores were not pretreated at all or partially due to an ineffective chelating agent preflush as well as a soaking time not long enough. The properties of this case are the same as the laboratory base case expect for the addition of $CaCl_2$. **Fig. 57** shows the maximum holdback pressure at different concentrations of $CaCl_2$ using polymer rheology data (Fig. 27). The results show the importance of the pretreatment stage to prevent syneresis and effectively seal the leakage pathways.

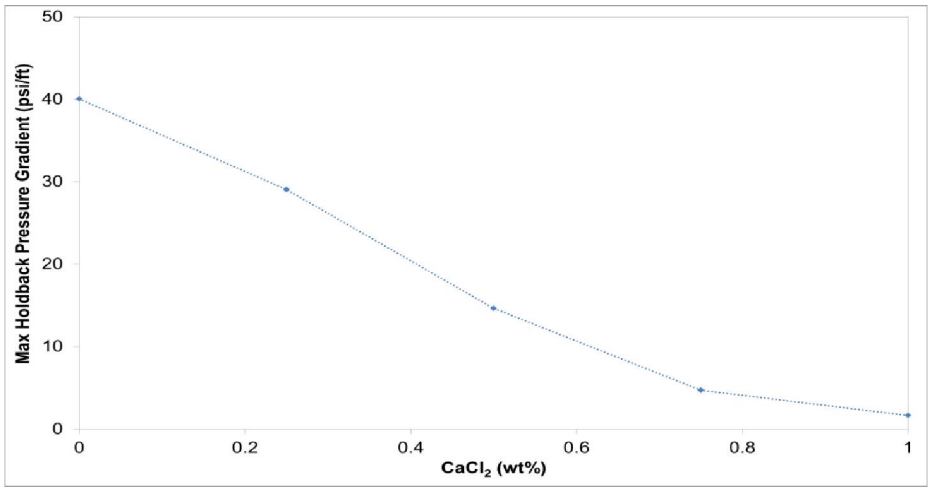

Fig. 57 – Effect of hardness (wt% $CaCl_2$) on the maximum holdback pressure gradient – water breakthrough test using simulation model considering the formation of gel deposit layer on cement surface.

3 Summary and conclusions

The novel sealant technology uses a pH-triggered mechanism well suited for wellbore cement in which polymer viscosification happens naturally and locally. The alkaline cement causes the increase in polymer pH and contributes to the effective transition of polymer solution into a yield stress gel. Compared to other applications (water shut-off, or conformance control), this wellbore sealant eliminates the need to account for a crosslinking agent and can develop significant gel strength at low relatively low concentrations. The injection of poly(acrylic acid) dispersion into an experimental cement fracture at ambient conditions have shown to successfully react with alkaline cement and seal the leakage pathways.

We developed experimental procedures and configurations to conduct experiments to test the capability of the polymer gel to block leakage pathways. Several experiments were performed to evaluate the polymer gel resistivity using brine injection. Moreover, the governing equations of the process were discussed and modeling procedure was explained. Polymer gel rheology and behavior were measured in laboratory experiments and formulations were developed to predict its behavior at different conditions. The simulation model was used to study the gelant flow through the fracture and the model was validated against laboratory experiments. Furthermore, several other experiments were performed to evaluate the polymer resistivity using acidic brine breakthrough tests. Additional experiments were conducted using CO_2 (low/high pressure) breakthrough tests. Finally, cement annulus bench tests were conducted using the setup analogous to real cement wellbores in shallow formations. The tests were done to evaluate the capability of pH-triggered gels to stop bulk phase CO_2 leaks. Several experiments and sensitivity analyses were performed to understand the effects of various parameters on the performance of polymer gel and to optimize the formulation in order to improve its performance.

Based on the well integrity application, experimental and simulation work done in this study conclude several key findings:

- Although many rheology tests have confirmed the ability of the polymer in developing significant yield stresses, an unexpected reaction occurred when tests were done with cement. Calcium ions contained in the cement leached out into the fracture and reacted with the polymer dispersion to form calcium precipitates. This reaction causes polymer syneresis in which water is expelled from the gel structure causing an irreversible shrinkage in volume. Syneresed gel is shown to be detrimental to the strength and long-term stability of the gel placement.

- The key to avoid the polymer syneresis is to inhibit the calcium ions in cement from reacting with the gel-in-place. It was found that a nano-clay particle known as Laponite could be mixed in polymer dispersion to desensitize ionic attractions and stabilize gel structure. This nano-composite hydrogel application was able to inhibit calcium syneresis and provide at least several months of effective seal; therefore, Laponite is considered to have potentials for improving gel longevity.

- Other chelating agents, such as EDTA and sodium triphosphate, were also used as syneresis inhibitors and are found to be effective at removing calcium by binding the ion to its structure before polymer injection. Despite the effectiveness of EDTA during visual observation of syneresis, the rapid reaction of polymer and EDTA during injection often resulted in irregular fluctuations in pressure and failed to maintain good polymer injectivity. In addition, hydrochloric acid was found to have little effect on calcium but have strong reaction with the iron content in cement, which often resulted in the appearance of both calcium syneresis and iron precipitation.

- Among the several syneresis inhibitors tested, it was determined that sodium triphosphate ($Na_5P_3O_{10}$) had the best performance when used as a pretreatment for cement cores. Cement cores pretreated with $Na_5P_3O_{10}$ not only inhibited polymer syneresis but also showed good injectivity and promising gel strength. The resulting holdback pressure gradients for pretreated cores were orders of magnitude higher than the few psi/ft measured for untreated cores and yielded better safety margin for the sealant design based on the 0.2-0.4 psi/ft required for a rising CO_2 leakage.

- In addition, multiple experiments showed that the calcium removal reaction of $Na_5P_3O_{10}$ and cement surface is very quick. This allowed pretreatment procedures to shorten from 24 hours to as brief as 10 minutes while maintaining desirable gel strengths; hence, use of $Na_5P_3O_{10}$ can greatly improve operational efficiency and results in less rig time.

- The development of gel strength is directly related to the static polymer shut-in time and the dehydration of reacted gel, as air bubbles form inside the fracture due to the slow reaction between residual $Na_5P_3O_{10}$ and the polymer. While the polymer gel could holdback as much as 15 psi/ft pressure gradient after only one hour of reaction, the matured/aged gel that has been shut-in for more than 5 weeks have a greater average gel holdback gradient of over 70 psi/ft.

- As expected, performance of the polymer gel system improves significantly as the effective fracture aperture gets smaller. A cement core subjected to high confining pressure to create a small fracture held as much as 3,000 psi/ft in pressure gradient when performed under supercritical CO_2 conditions. The result of gel strength was seen to improve exponentially as effective apertures were less than 300 microns, while there was less correlation in larger aperture ranges.

- Contrary to what had been expected, the effect of the type of holdback fluid used is negligible on the initial breakthrough from multiple tests. This is due to the nature of the small fractures where the contact (reaction surface area) of the holdback fluid with reacted gel is extremely small; the fluid breakthrough is mainly caused by the pressure gradient increase. However, once the gel is broken through by pressure, the effect of holdback fluid type was apparent. The acidic (lower pH) fluid that is contacting more surface area of gel was then able to reverse the pH-triggered gelling mechanism and quickly dissolve the gel in place.

- Multiple experiments done in ambient conditions have proven that the pH-sensitive polymer gel system has sufficient gel strength to block 10-100 psi/ft of pressurized fluids. This can conclude the effectiveness of its application for sealing leakage pathways in shallow formation (up to 70°C in subsurface temperature). Furthermore, the result from the CO_2 breakthrough tests in small fracture apertures show that the injected polymer gel can hold 100-1,000 psi/ft of pressure gradients under supercritical condition and will be more than sufficient to hold the required few psi/ft for an uprising buoyant CO_2 plume from a leaky storage well.

- The Carbopol 934 properties are dependent on polymer concentration, pH, and salinity. rheological behavior of Carbopol 934 was investigated for ranges of polymer concentrations of 1-3 wt%, pH of 2-13, and salinity of 0.5-3 wt% NaCl.

- Flow curves, the shear stress versus shear rate, were generated for different concentrations of polymer. From the flow curve, required parameters for modeling of the process were obtained. The flow curve of the shear stress versus shear rate of the polymer gelant is well-described by the Herschel-Bulkley equation.

- The underlying flow and transport formulation of the process was provided. The sets of equations were further non-dimensionalized to better understand the significance of various physical effects and to facilitate the scaleup to larger scales.

- Simulation models were developed capable of modeling flow with non-Newtonian fluid behavior and particle transport from the cement surface and through the fracture. Calculation flow chart was presented to model the experiments. The experiments were polymer injection and water breakthrough tests. The simulation results are in line with experiments. The simulated pressure gradient, steady-state flow rate, and time to reach to steady-state flow are comparable with the observed values for the polymer injection and water breakthrough tests.

- It was hypothesized that as the flowing fluid pH increases above the critical pH, the solid microgel particles will swell. Some of the swollen particles will deposit on cement surface. The deposited swollen microgels will form a gel layer. Hydroxide ions will still diffuse through

the gel layer, but at a rate much slower than that through the flowing fluid. The simulation model was updated with consideration of a gel deposit layer on cement surface. The new model predicts higher values of pressure gradients because hydroxide ions dispersed less to the bulk as the gel deposit layer forms on the cement surface. The laboratory data points of pressure gradients cover a wide region because of the experimental uncertainties including prediction of fracture aperture size. The theoretical pressure gradient was also calculated using the polymer rheology data. The comparison of data shows satisfactory results obtained using the simulation model.

- Additional simulations were performed at different fracture aperture sizes and polymer concentrations to understand the effect of fracture aperture on the holdback pressure. The trend is alike what observed in the experiments with various fracture aperture sizes. The holdback pressure increases at higher polymer concentrations. The results are useful to decide on polymer concentration if the estimated average aperture size of the target region to be sealed is known.

pH-sensitive polymer-gel systems have been well-studied for various enhanced oil recovery applications; however, little is known or discussed about its novel application in enhancing wellbore integrity. More work is necessary to improve the performance and feasibility of this sealant technology. It is highly recommended for future studies to focus on the following:

Lab-scale corefloods at reservoir conditions: Some corefloods performed in this study have indicated the potential use of the polymer sealant above ambient conditions. However, supercritical CO_2 and many other fluids are likely stored in deeper formations under high pressure, high temperature conditions. Additional polymer corefloods should be conducted in Hassler coreholders to evaluate the thermal stability (above 70°C), pressure-induced shrinkage, and the aging of gel at higher pressure and temperature settings.

Field-scale applications in shallow wells: The polymer-gel sealant is presumably ready for field-scale tests in shallow wells. Preparation work should be carried out to thoroughly investigate in leakage conditions and fracture patterns in the cement wellbore. There will most likely be technical risks that require concern; hence, new laboratory experiments should be specifically designed to evaluate those problems.

REFERENCES

Albonico, P. and Lockhart, T.P. 1997. Stabilization of polymer gels against divalent ion-induced syneresis. *Journal of Petroleum Science and Engineering* **18**(1) 61-71.

A-sasutjarit, R., Sirivat, A., and Vayumhasuwan, P., 2005. Viscoelastic properties of Carbopol 940 gels and their relationships to Piroxicam diffusion coefficients in gel bases. *Pharmaceutical Research* **22**(12): 2134-2140.

Barnes, H.A. 1999. A brief history of yield stress. *Appl. Rheol.* **9**: 262-266.

Barnes, H.A. 1999. The yield stress—a review—everything flows? J. *Non-Newtonian Fluid Mech.* **81**: 133–178.

Bird, R.B., Armstrong, R.C., and Hassager, O., 1987a. Dynamics of Polymeric Liquids. Volume 1: Fluid Mechanics. Wiley Intersci., New York.

Bird, R.B., Curtiss, C.F., Armstrong, R.C., and Hassager, O., 1987b. Dynamics of Polymeric Liquids. Volume 2: Kinetic Theory. Wiley Intersci., New York.

Carbopol®, Cross-linked Polyacrylate Polymer, the Lubrizol Corporation.

Cloitre, M., Borrega, R., Monti, F., and Leibler, L. 2003. Structure and flow of polyelectrolyte microgels: from suspensions to glasses. *C. R. Physique* **4**: 221-230.

COMSOL Multiphysics 2015. User Manual. Comsol Inc.

Dusseault, M.B., Gray, M.N., and Nawrocki, P.A. 2000. Why Oilwells Leak: Cement Behavior and Long-Term Consequences. Presented at the SPE International Oil and Gas Conference and Exhibition, Beijing, China, 7-10 November. SPE-64733.

Guo, H., Aziz, N.I., and Schmidt, L.C., 1993. Rock fracture-toughness determination by the Brazilian test. *Engineering Geology* **33**(3):177-188.

Gutowski, I.A., Lee, D., de Bruyn, J.R., and Frisken, B.J. 2012. Scaling and mesostructure of Carbopol dispersions. *Rheol. Acta* **51**(5): 441-450.

Helfrich, K.R. 1995. Thermo-viscous fingering of flow in a thin gap: a model of magma flow in dikes and fissures. *J. Fluid Mechanics* **305**: 219-238.

Ho, J.F., Patterson, J.W., Tavassoli, S., Shafiei, M., Balhoff, M.T., Huh, C., Bommer, P.M., and Bryant, S.L. 2015. The use of a pH-triggered polymer gelant to seal cement fractures in wells. Presented at the 2015 SPE Annual Technical Conference and Exhibition held in Houston, Texas, U.S.A., 28-30 September. SPE-174940-MS.

Ho, J.F. 2015. *The use of a pH-triggered polymer gelant to seal cement fractures in wells*. MS thesis, The University of Texas at Austin, Austin, Texas, U.S.A. (December 2015).

Huh, C., Choi, S.K., and Sharma, M.M. 2005. A Rheological Model for pH Sensitive Ionic Polymer Solutions for Optimal Mobility. Presented at the SPE Annual Technical Conference and Exhibition held in Dallas, Texas, U.S.A., 9 – 12 October. SPE-96914.

Milanovic, D. and Smith, L.2005. A Case History of Sustainable Annulus Pressure in Sour Wells – Prevention, Evaluation and Remediation. Prepared for presentation at the SPE High Pressure/High Temperature Sour Well Design Applied Technology Workshop, The Woodlands, Texas, U.S.A., 17 - 19 May. SPE-97597.

Patterson, J.W. 2014. *Placement and performance of pH-triggered polyacrylic acid in cement fractures*. MS thesis, The University of Texas at Austin, Austin, Texas, U.S.A. (May 2014).

Roberts, G.P. and Barnes, H.A. 2001. New measurements of the flow curves for carbopol dispersions without slip artifacts. *Rheol. Acta* **40** (5): 499–503.

Shafiei, M., Bryant, S.L., Balhoff, M.T., Huh, C., and Bonnecaze, R., 2016. Hydrogel Formulation for Sealing Cracked Wellbores for CO_2 Storage. *Journal of Rheology* (paper in preparation).

Tavassoli, S., Ho, J.F., Shafiei, M., Balhoff, M.T., Huh, C., Bommer, P.M., and Bryant, S.L. 2016. A Novel Remedy to Wellbore Leakage: Experimental and Numerical Study. (paper in preparation).

Tongwa, P., Nygaard, R., and Baojun, B., 2013. Evaluation of a nanocomposite hydrogel for water shut-off in enhanced oil recovery applications: Design, synthesis, and characterization. *Journal of Applied Polymer Science* **128**(1): 787-794.

Watson, T.L., and Bachu, S. 2007. Evaluation of the Potential for Gas and CO2 Leakage Along Wellbores. Presented at the E&P Environmental and Safety Conference, Galveston, Texas, U.S.A., 5-7 March. SPE-106817.